Ore Geology Reviews 72 (2016) 459–484

Contents lists available at ScienceDirect

Ore Geology Reviews

journal homepage: www.elsevier.com/locate/oregeorev

Oxidized and reduced kaolin fan deposits: Their sedimentological–mineralogical facies and physical–chemical regime (North-Bavarian Kaolin Mining District, Germany)

Harald G. Dill [a,*], Stephan Kaufhold [b], Angela Ehling [c], Jörg Bowitz [d]

[a] Gottfried Wilhelm Leibniz University, Welfengarten 1, D-30167 Hannover, Germany
[b] Bundesanstalt für Geowissenschaften und Rohstoffe, D-30631 Hannover, P.O. Box 510163, Germany
[c] Bundesanstalt für Geowissenschaften und Rohstoffe, D-15693 Berlin, Wilhelmstraße 25-30, Germany
[d] Schönwalder Straße 60, D-13585 Berlin, Germany

ARTICLE INFO

Article history:
Received 10 June 2015
Received in revised form 31 July 2015
Accepted 6 August 2015
Available online 14 August 2015

Keywords:
Kaolin
Fan deposits
Physical–chemical regime
Sedimentological–mineralogical facies
Mesozoic
SE Germany

ABSTRACT

The kaolin-fan deposits under consideration are sedimentary in origin and they bridge the gap between residual kaolin deposits proximal to the fan apex in crystalline basement rocks and syn(dia)genetic sandstone-hosted kaolin deposits on the fan apron. The "kaolin ore beds" on the other hand, developed in an arenaceous braided-river drainage system (bed load >>> suspended load deposits), reworking into secondary kaolin deposits that took place either intraformationally during the evolution of the kaolin fan deposits or epigenetically after unroofing of the kaolin deposits in high-sinuosity drainage systems passing, locally, into ephemeral lakes and mud flats (suspended load > bed load deposits). The reference type for kaolin fan deposits has been studied in terrigeneous sediments which are largely mined at Hirschau–Schnaittenbach, along the Western edge of the Bohemian Massif, SE Germany.

The fan deposits formed under alternating wet and dry subtropical climatic conditions during the early Triassic. Different intensities of uplift in the hinterland and the frequency of tectonic quiescence to tectonic pulse had a strong impact on the paleogradient, facies and hydrography of the kaolin fan deposits, resulting in the build-up of oxidized kaolin fans (OKF) and reduced kaolin fans (RKF). The OKF provide favorable conditions for the accumulation and preservation of kaolin deposits of economic potential, due to a low paleogradient and a continuous rate of uplift. The opposite is the case in the RKF that formed more proximal to the initial residual kaolin deposits and, more basinward, grade into sandstone-hosted (non)-sulfidic faciesbound Pb deposits that were targeted upon during exploration campaigns in the study area.

The mineral association of the kaolin fan deposits has been categorized as follows: the allochthonous heavy minerals are zircon, tourmaline, apatite, monazite, xenotime, rutile, garnet, titaniferous magnetite, and ilmenite. They do not significantly vary between OKF and RKF. The autochthonous heavy minerals show strong contrasts in their heavy mineral suites. The RKF are enriched in sulfides and arsenides, which can be deleterious for the kaolin raw material and exclude its use for special final products (anatase, hematite, galena, sphalerite, marcasite, pyrite, bravoite (Ni pyrite), "limonite", goethite, Ag–Cu–Ni–As sulfides, and barite). The OKF are rather poor in accessory minerals and contain anatase, hematite, and APS minerals. The latter are geo-acidometers (marker minerals for low pH) and considered as an ore guide to high-potential target areas for kaolin. The allochthonous light minerals quartz and K feldspar are common to both fan types and were only in parts affected by kaolinization, whereas plagioclase has been decomposed to completeness. Autochthonous light minerals quartz, chalcedony (carnelian), and calcite are exclusive to the RKF, where silcretes and calcretes evolved in those stratigraphic units which in the OKF only brought about Ca, Fe and Ti anomalies. The OKF have a significant edge over the RKF in terms of kaolin quality and kaolin exploitation (providing less mechanical wear on LHD [load–haul–dump machinery] machinery). Allochthonous phyllosilicates have a more widespread occurrence in the RKF with muscovite, biotite and chlorite most common in the lowermost kaolin beds. By quality there is not much difference among the autochthonous phyllosilicates of the OKF and RKF. Kaolinite-group minerals, illite, smectite, and an illite–smectite mixed-layer are present in both types, but kaolinite-group minerals prevail in the OKF, with a downward-increasing trend of dickite. By contrast the amount of smectite and smectite–illite mixed layers increases at the expense of kaolinite upward in the stratigraphy.

* Corresponding author.
E-mail address: haralddill@web.de (H.G. Dill).
URL: http://www.hgeodill.de (H.G. Dill).

http://dx.doi.org/10.1016/j.oregeorev.2015.08.003

The evolution of the kaolin fan deposits can be subdivided into six stages. Each stage is representative of a peculiar process which translates into concentration, preservation and destruction of kaolin: stage 1 weathering and the formation of a kaolin regolith (constructive), stage 2 transport, deposition synsedimentary to early-diagenetic kaolinization (constructive + preserving), stage 3 synsedimentary to early-diagenetic smectitization of kaolin (faciesbound Pb mineralization only in the RKF) (preserving + destructive), stage 4 late-diagenetic kaolinization and formation of dickite (preserving + constructive) (not in RKF), stage 5 epigenetic unconformity-related Cu–Ag–Ni–As–Ba mineralization (vaguely expressed in the OKF) (preserving), and stage 6 unroofing, erosion and redeposition of kaolin (only in the OKF) (destructive).
During the study a PIMA device has proven in this type of kaolin deposit to be an efficacious tool for capturing digital data in the field of exploitation and exploration of industrial minerals for the identification and quantification of clay minerals (quality control).

1. Introduction

Kaolin, pertaining to the industrial-mineral group, is a rock in which the three polymorphs kaolinite (triclinic), dickite (monoclinic) and/or nacrite (monoclinic) of the kaolinite-group (kandite-group), including halloysite, prevail over the associated rock-forming minerals. It has been widely demonstrated that these fine-grained rocks can form during supergene and hypogene alteration from a great variety of parent rocks (Bristow, 1977; Kromer, 1980; Weaver, 1989; Dill et al., 1997; Psyrillos et al., 1998; Abeysinghe and Fetherston, 1999; Cravero et al., 2001; Scott and Bristow, 2002; Alü Sayin, 2007; Domínguez et al., 2010; Fernández-Caliani et al., 2010; Kadir and Erkoyun, 2013; Grecco et al., 2012).

In the current study focus is laid on sedimentary rocks undergoing near-surface and shallow-burial kaolinization along the western edge of the Bohemian Massif and its Foreland (Fig. 1a,b). The aforementioned processes engendered the largest kaolin mining district in Central Europe, in SE Germany, in the Hirschau–Schnaittenbach region.

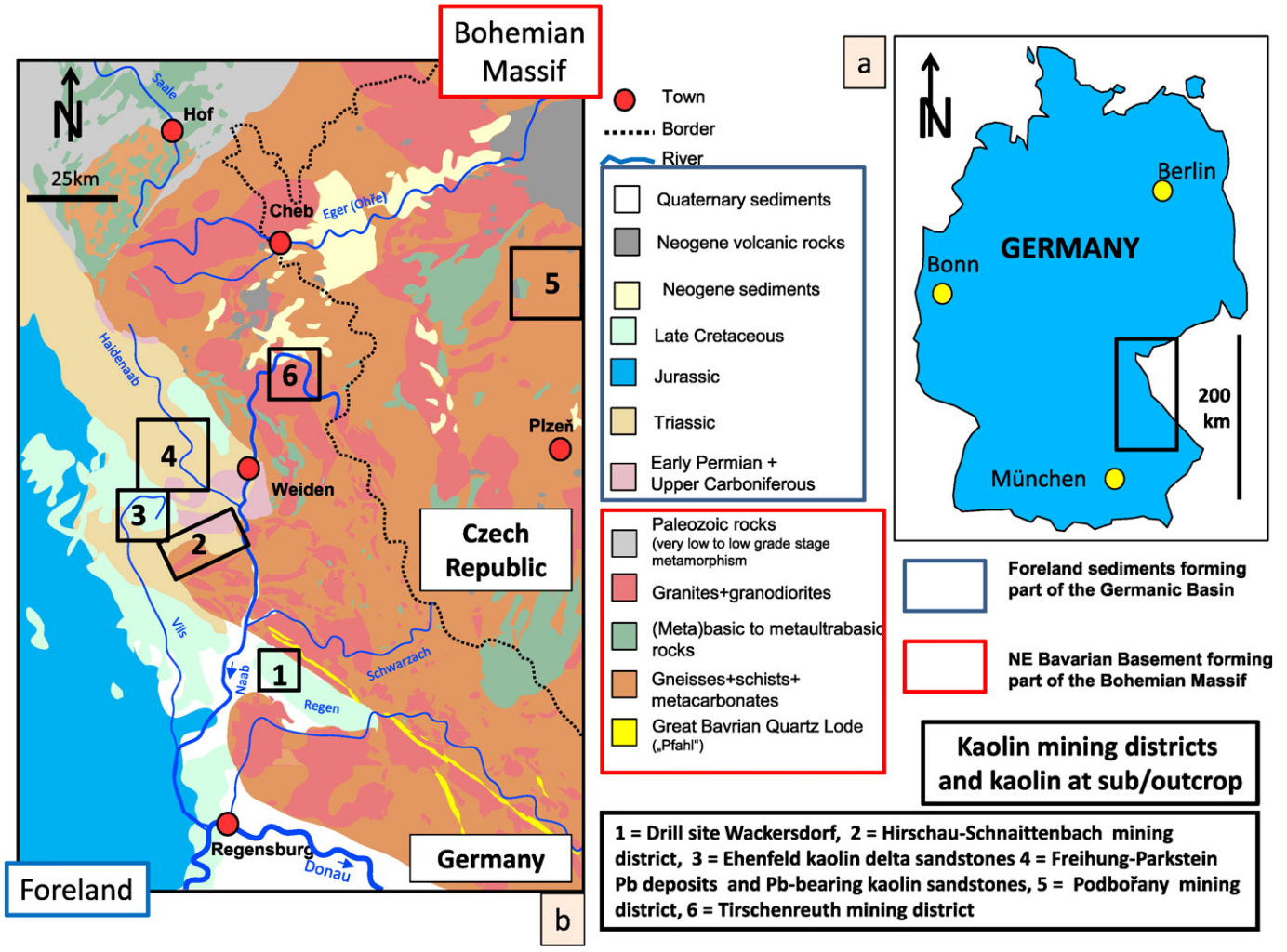

Fig. 1. The geological setting and position of the kaolin deposits along the western edge of the Bohemian Massif and within its foreland. a) The position of the working area along the Czech–German border. b) The geology along the western edge of the Bohemian Massif representative of the NE Bavarian Basement and the Upper Carboniferous through Quaternary platform sediments in the foreland forming part of the Germanic Basin. The framed area in Fig. 1a denotes the position of Fig. 1b. The black rectangles mark the sites abundant in kaolin which were studied and referred to in the text. Positioning is based upon Dill et al. (2008a,b).

Kaolin is not only exposed in vast open pits, targeted upon for pervasively kaolinized arkoses but also hit in several drill holes underneath a huge pile of Mesozoic platform sediments, providing a good coverage to study the origin of kaolin deposits from the present-day landscape down to 350 m depth (Köster, 1974; Störr, 2002, 2006; Dill and Klosa, 2011; Dill and Berner, 2014) (Figs. 1, 2). Wackersdorf is not a deposit in the commercial sense, because it was found at a depth of approx. 300 m, but has to be denominated as a "blind kaolin ore body".

The results obtained throughout the current studies in SE Germany have an edge over investigations focusing only on samples taken at

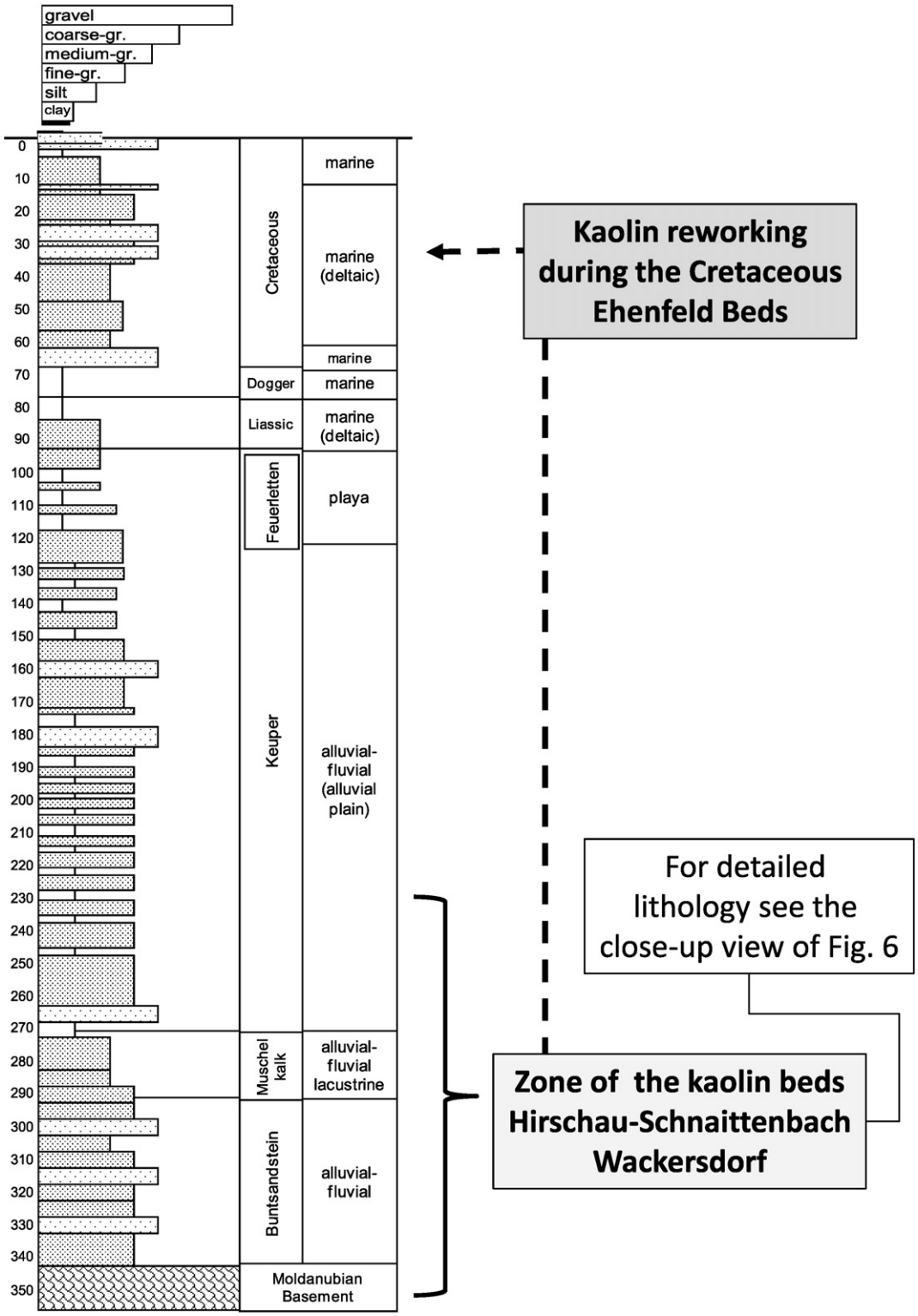

Fig. 2. Simplified litholog (variable-width column) of the Wackersdorf drill hole, covering the rock section from the early Triassic Buntsandstein through the Late Cretaceous foreland sediments which unconformably rest on altered basement rocks of the Moldanubian Zone. For grain size variation see the key on top of the litholog and for interpretation of the depositional environment the column on the right-hand side (for stratigraphic fine-tuning and a more detailed analysis of the depositional environment of the kaolin beds see Fig. 6). The vertical bar denotes the stratigraphic section most intensively kaolinized. Depth is given in meter. The stippled line marks the reworking of Triassic kaolin fan deposits into the Late Cretaceous Ehenfeld Beds.

outcrop and can be used in two different ways. First of all, the issues discussed in the current publication are applicable to the sediment-hosted kaolin mineralization located elsewhere within the same depth interval, *e.g.*, the Czech Republic, France, USA, and Great Britain and may contribute to fine-tune the genesis in these mining regions (Wilson and Jiranek, 1995; Elzea Kogel, 2002; Koneshloo et al., 2005; Bruke, 2006). Secondly, the geophysical data collected in the course of this study by the SWIR technique are useful for the applied part of economic geology, while trying to find either new kaolin deposits by drilling operation or conducting grade and quality control of run-off mine kaolin by capturing digital data in the field (Dill et al., 2015). To give full particulars of the current study, the scope can be highlighted by the following five bullet points:

- using the entire range of geoscientific disciplines (sedimentary petrography, structural geology, mineralogy, geophysical logging and chemistry) to decipher the build-up, preservation and denudation of kaolin deposits in terrigeneous sedimentary environment
- determining the evolution of kaolinization in Permo-Mesozoic platform sediments and in their crystalline basement rocks lying immediately underneath
- discussing the physical–chemical regime during the various stages of kaolinization and its impact on the variation of the clay mineral assemblage
- comparing physical methods on-site with laboratory techniques to test their effectiveness as capturing digital data in the field or during drilling campaigns
- comparing of the newly-described type of kaolin deposit with other sediment-hosted types and its integration into existing classification schemes of mineral deposits.

Our principle goal is to broaden the knowledge of using kaolin from the upstream part, in other words, elaborating exploration models and going beyond studies of applied clay mineralogy and processing as they were referred to by Murray (2000, 2007) in his overviews (Table 1).

During the study of the genesis of the Hirschau–Schnaittenbach kaolin deposits which currently are mined by two companies, Amberger Kaolinwerke/AKW–Kick (reserves lasting for 40 years/precise mining data are proprietary) and Dorfner (mining data are proprietary), these kaolin deposits are also compared with neighboring sediment-hosted kaolin accumulations. One type of reference deposit was emplaced higher up in the stratigraphic sequence at Ehenfeld, Germany, and the other zones of kaolinization are straddling the boundary between the crystalline basement rocks and its Mesozoic overburden on Czech and German territories (Fig. 1b).

2. Field and laboratory methods

In the aftermaths of the geological field work, which runs from mapping, drill core and drill cutting examinations, through sedimentological studies at outcrop, 184 samples from drill cores and from percussion drillings were taken for follow up mineralogical and chemical investigations in the laboratory.

Samples were sieved and the grain size fraction 63 to 600 μm was used for follow-up HM analyses. During routine analyses, the HM (density > 2.9 g/cm^3) were extracted by means of Na-polywolframate. After removal of iron oxide coatings with Na dithionite, translucent HM were mounted on glass disks using Canada balsam and identified under the petrographic microscope, considering between 200 and 300 grains per sample for mineral analysis if present. X-ray diffraction analysis of some particles supplemented the petrographic studies.

XRD patterns were recorded using a Philips X'Pert PW3710 Θ–2Θ diffractometer (Cu-Kα radiation generated at 40 kV and 40 mA), equipped with a 1° divergence slit, a secondary monochromator, a point detector and a sample changer (sample diameter 28 mm). The samples were investigated from 2° to 80° 2Θ with a step size of 0.02° 2Θ and a measuring time of 3 s per step. For specimen preparation, the top loading technique was used.

SEM–EDX is an important supplement to XRD. No sputter coater was used prior to SEM–EDX analyses by means of a QUANTA 600 FEG equipped with a GEMINI EDX system because all analyses were carried out under low-vac-chamber conditions (1 to 10 mbar).

Major and trace elements were analyzed by X-ray fluorescence spectrometry (XRF) and by ICPMS (Li and Be). The chemical composition of powdered samples was determined using a PANalytical Axios and a PW2400 spectrometer. Samples were prepared by mixing with a flux material (Lithiummetaborate Spectroflux, Flux No. 100A, Alfa Aesar) and melting into glass beads. The beads were analyzed by wavelength dispersive X-ray fluorescence spectrometry (WD-XRF). To determine loss on ignition (LOI) 1000 mg of sample material was heated to 1030 °C for 10 min.

The CEC was measured using the Cu-triethylenetetramine method (Meier and Kahr, 1999). The method was applied to the 1–2 mm fraction with different reaction times. Standard reaction time for the powders is 2 h shaking in an end-over-end shaker. The 1–2 mm samples were additionally investigated with respect to the CEC after 48 h shaking followed by 10 min ultrasonic treatment and finally after an additional 72 h shaking followed by an additional 10 min ultrasonic treatment.

As some minerals may be identified much better, using their spectroscopic signature, infrared spectroscopy was carried out in addition to the routine XRD. For measuring mid (MIR) infrared spectra the KBr pellet technique (1 mg sample/200 mg KBr) was applied. Spectra were collected on a Thermo Nicolet Nexus FTIR spectrometer (MIR beam splitter: KBr, detector DTGS TEC; FIR beam splitter: solid substrate, detector DTGS PE). The resolution was adjusted to 2 cm^{-1}. Spectra were recorded before and after the drying of the pellets at 150 °C and vacuum. Only the spectra of the dried pellets are shown.

Another method making use of the short wave length in the range 1300 to 2500 nm of the IR electromagnetic spectrum (SWIR) was used. Infra-red analysis, involving acquisition and first-hand interpretation of data was carried out with a portable battery-driven infrared mineral analyzer (PIMA) from Integrated Spectronics Pty Ltd. The system was calibrated to wave length and reflectance for routine data acquisition. A special software package "PimaView version 3.1" from Integrated Spectronics Pty Ltd. was used to automatically analyze the IR sensitive minerals. It helps in identification and enables the sampler to perform a (semi-)quantitative determination of the major IR-sensitive components of kaolin in the various samples. The theoretical basis of this method was laid by Herrmann et al. (2001). When a rock is illuminated by an IR-light source certain wavelengths of the light are absorbed by the rock-forming minerals as a result of sub-molecular vibrations. Bending and stretching of molecular bonds in the mineral is especially strong in minerals containing hydroxyl ($(OH)^-$) and carbonate ($(CO_3)^{2-}$) complexes. It may also successfully be applied to sulfates or phosphates that play an important part among non-metallic commodities too. The spectrometer measures the reflected radiation from the surface of rocks and minerals in the short wavelength infrared (SWIR). Duke (1994) and Clark (1999), also provided an outlook into advanced level studies using remote sensing and Dill (2003b) showed some case histories from Mongolia and Thailand on how to use this method from the exploration of non-metallic deposits.

3. Geological setting

3.1. The basement rocks

The basement rocks exposed adjacent to the Permo-Triassic foreland sediments in the Hirschau–Schnaittenbach area and hit underneath the platform sediments in the well at Wackersdorf belong to the

Table 1
Lithology and mineralogy of kaolin deposits (bright brown) under study and the interpretation of their environment of deposition, the source area and the evolution of the reduced and oxidized kaolin fans (yellow). The green boxes show the position of the two reference types of fan deposits. The sections, where the various topics are referred to in this study are given in brackets. Boxes framed with bold-faced lines refer to topics genetically related with each other.

Items + issues	Hirschau-Schnaittenbach-Type "oxidized kaolin fan"	Wackersdorf-Type "reduced kaolin fan"
Lithology (terrigenous)	Embedded kaolin-bearing sediments - conformity-related Tabular and trough-shaped cross-bedding, coarse to fine-grained feldspar arkoses with sporadic discontinuous clay bands. Gravel only disseminated. Lower contact gradual into more massive conglomeratic arkoses, upper contact gradual, cyclothems common	Covered kaolin regolith with sedimentary overburden-unconformity-related Sediments similar to Hirschau-Schnaittenbach. Multicolored arkoses, with quartz pebbles, calcretes and silcretes. FU- and CU cycles. Direct contact to strongly kaolinized metamorphic basement rocks
Lithology (chemical)	Anomalies of Ca, Fe and Ti	Duricrusts of Ca and Si Silcretes, calcretes and calcareous cement
Heavy minerals allochthonous	Rutile, tourmaline, monazite, xenotime, zircon, magnetite	Zircon, tourmaline, apatite, monazite, xenotime, rutile, garnet, titaniferous magnetite, ilmenite
Heavy minerals autochthonous	Anatase, hematite, APS minerals	Anatase, hematite, galena, sphalerite, marcasite, pyrite, bravoite (Ni pyrite), „limonite“ , goethite, Ag-Cu-Ni-As sulfides, barite
Light minerals allochthonous	Quartz, K feldspar	Quartz, K feldspar
Light minerals autochthonous		Quartz, chalcedony (carnelian), calcite
Phyllosilicates allochthonous	Rare biotite, muscovite	Biotite, chlorite common in the lowermost kaolin beds, muscovite
Phyllosilicates autochthonous	Kaolinite-group minerals, dickite, illite, smectite, illite-smectite mixed-layer	Kaolinite-group minerals, illite, smectite, illite-smectite mixed-layer
Preferred *loci* of kaolinization and reworking	Kaolinization within the bed-load deposits and reworking into suspended-load deposits	Kaolinization in-situ within the regolith and reworking into bed-load and suspended-load deposits
Depositional environment (terrigenous) (sect 5.1)	Alluvial-fluvial fan with braided stream drainage systems (arenaceous >>>gravelly), Consequent evolution of a transport system from regressive (kaolin concentration) to prograding (kaolin preservation)	Alluvial-fluvial fan with braided stream drainage systems (arenaceous >gravelly), Intermittent evolution of drainage and transport system with frequent relapses and facies changes from prograding (kaolin concentration) to regressive (kaolin denudation)
Depositional environment (chemical) (sect. 5.1)	Mud flats with relic paleosols	Mud flats with small ephemeral lakes and ponds
Source rock and transport (sect 5.2)	H-T metamorphic rocks + intermediate to felsic volcanites Distal (apatite-out) 5 to 10 km distance between source and reservoir rock	H-T metamorphic rocks + intermediate to felsic volcanites Proximal (apatite-in) reservoir rock on top of source rock
Weathering and the formation of a kaolin regolith (sect. 5.3.1) -constructive-	Residual kaolin:eroded age: pre Early Triassic	Residual kaolin: preserved age: pre Early Triassic pH: 6 to 8 alternating dry and wet savannah climate

(*continued on next page*)

Table 1 (*continued*)

Transport and deposition (sect. 5.3.2) -constructive- -preserving-	Synsedimentary to early-diagenetic kaolin age: Early Triassic pH: 1.5 to 6 Eh: > 0 volts Silica activity constant Deposition and preservation, consequent	Synsedimentary to early-diagenetic kaolin age: Early Triassic pH: 6 to 11 Eh: locally < 0 volts Silica activity fluctuating Erosion, deposition and preservation cyclic
Alteration I of kaolin (sect. 5.3.3) -preserving- -destructive-	Synsedimentary to early-diagenetic smectitization of kaolin age: Early to middle Triassic pH: 7 to 9 Eh: > 0 volts	Synsedimentary to early-diagenetic smectitization of kaolin age : Early to middle Triassic pH: 7 to 9 (locally exceeding pH 9) Eh: locally < 0 volt Faciesbound Pb sulfide mineralization Detrimental to the run-off mine kaolin
Alteration II of kaolin (sect. 5.3.4) -preserving- -constructive-	Late-diagenetic kaolinisation and formation of dickite age: post-middle Triassic (?) pH: 1.5 to 6 (organic fluids) Eh: > 0 volts Silica activity constant	Not observed
Mineralization in kaolin (sect. 5.3.5) -preserving-	Epigenetic unconformity-related Ag anomaly age: early Cretaceous No physical-chemical regime analysis	Epigenetic unconformity-related mineralization Cu-Ag-Ni-As-Ba age: early Cretaceous T: < 200°C pH: fluctuating around 7 Eh: < 0
Exhumation and redeposition (sect. 5.3.6) -destructive-	Unroofing, erosion and redeposition of kaolin age: late Cretaceous No physical-chemical regime analysis	Not observed

Moldanubian Zone of the Central European Variscides, the morphological expression of which in the study area is the NE Bavarian Basement (Fig. 1). An overview of this geodynamic zone has been given among others by Matte (2001) and Raumer von et al. (2003). The Moldanubian zone represents a stacked pattern of nappes of medium to high-grade metamorphic rocks which were superimposed onto each other during the late Variscan deformation (Fig. 1). The basement rocks in the Moldanubian zone consist of paragneisses derived from greywackes and arenites and of meta(ultra)basic rocks, metabiolites, marbles and calcsilicates interpreted as a volcano-sedimentary series. During the Late Carboniferous subsequently to the Variscan deformation granites intruded into these basement rocks (Fig. 1). The granites intruded into biotite gneisses yielded U–Pb ages between 321–329 Ma (Siebel et al., 2005).

3.2. The foreland sediments

The foreland sediments in the Wackersdorf drill hole, which is the deepest well under study for kaolin and whose data are reported in this publication, cover the Mesozoic stratigraphy from the Lower Triassic Buntsandstein through to the Late Cretaceous, excluding the upper Jurassic and the Early Cretaceous as the region has emerged as dryland (Figs. 1, 2). During the Lower Triassic Buntsandstein, equivalent to the Induan to Olenenkian, arenaceous and argillaceous red bed sediments were deposited in the SE part of the Germanic Basin (Aigner and Bachmann, 1992) (Figs. 2, 3a, Table 2). They formed in a continental depositional environment. The middle Triassic Muschelkalk beds, laid down contemporaneously with the Anisian to lower Ladinian beds in the Tethys basin, are representative of the only marine incursion during the Triassic into the Germanic Basin. This incursion described by Aigner and Bachmann (1992) for the central part of the basin, has been of little effect on the area under study in NE Bavaria, where the Muschelkalk (= shellfish-bearing limestone) is lithologically represented by a rather monotonous series of arenaceous to conglomeratic siliciclastic rocks, called Muschelsandstein (= shellfish-bearing sandstone) (Figs. 2, 3b) (Gudden, 1975) (Table 2). Compared with the preceding Muschelkalk, the upper Ladinian to Rhaetian Keuper in the Germanic Basin is representative of a relapse into a more continental environment (Reinhard and Ricken, 2000; Hornung and Aigner, 2002) (Figs. 2, 3c). By the beginning of the Jurassic the epicontinental Liassic sea encroached upon the upper Keuper Feuerletten playa, leaving behind dark claystones, black shales and sandstones (Meyer and Schmidt-Kaler, 1996). The Middle Jurassic (Dogger) is similar as to environment of deposition in the area under consideration but contains coarser-grained sandstones than its Liassic predecessor (Fig. 2). In places, oolitic Minette ironstones accumulated in a near-shore marine environment (Siehl and Thein, 1989). During Late Jurassic and Early Cretaceous the study area was emerged as illustrated by the lithology/mineralogy which reveal a marked hiatus around a drill depth of 70 m (Fig. 2). While the previous marine incursions flooded the basin from the NW, during the late Cretaceous (Cenomanian through upper Turonian) another incursion of the sea occurred from the Alpine foreland. The marine flooding was basin guided by the "Regensburg Strait", a narrow embayment that stretched NNW–SSE along the boundary of the present-type uplifted crystalline rocks of the Bohemian Massif — for the occurrence of the Cretaceous beds see also Fig. 1b (Meyer and Mielke, 1993). During the Neogene, in the northern part of the study area sedimentary sequences evolved in a large coal-bearing depression extending across the Czech–German border into northern Bohemia (Zitzmann, 1981). Volcanic activity accompanying this basin subsidence was constrained geochronologically at

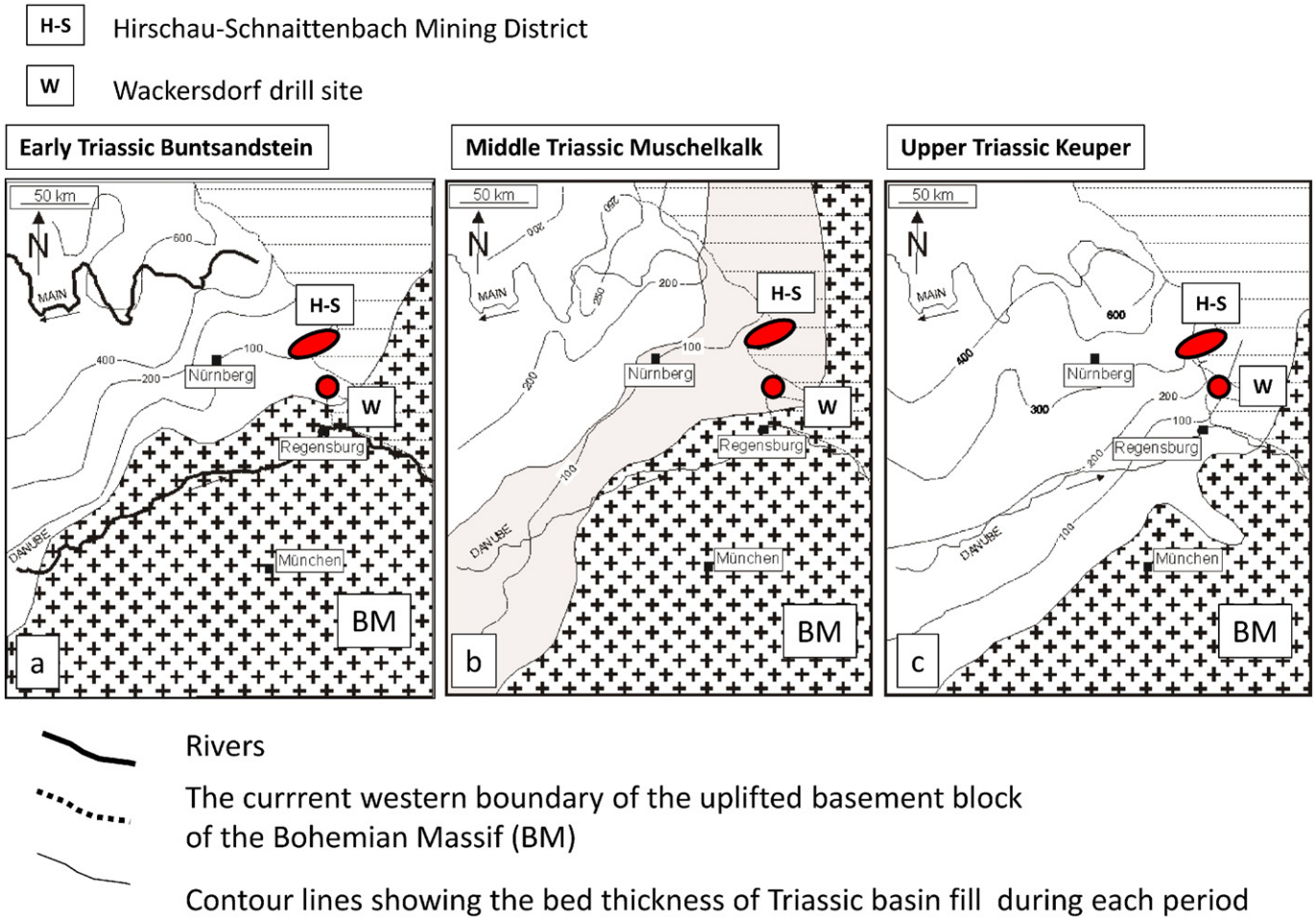

Fig. 3. Paleogeographic sketch maps of the Triassic series in SE Germany and the kaolin mineralization in the foreland sediments under study (red round and ellipsoidal areas). The paleogeography has been modified from the official map "Geologische Karte 1: 500 000 Bayern" issued by the former Geological Survey of Bavaria. a) Early Triassic Bunter Series (Buntsandstein). b) Middle Triassic Muschelkalk (the shaded area denotes the arenaceous facies of the Muschelkalk along the SE boundary of the Germanic Basin). c) Upper Triassic Keuper.

Table 2
Stratigraphic table listing the local terms of relevance for the kaolinization together with the internationally applied terms to correlate the kaolin fan deposits under study with sedimentary kaolin deposits elsewhere.

Period	Faunal stages	Stratigraphic terms in Central Europe		Local terms used during mapping and mining	
Triassic	Ladinian	*Lower Middle Keuper*			"Benker Sandstein"
		Lower Keuper			
	Anisian to lower Ladinian	*Muschelkalk*			
	Induan to Olenenkian	*Buntsandstein*	Upper Buntsandstein		
			Middle Buntsandstein	Upper Hauptbuntsandstein	
				Lower Hauptbuntsandstein	"Kulmbacher Konglomerat"
Precambrian		*Moldanubian*			

the interval from 29 Ma to 19 Ma–late Oligocene to early Miocene (Huckenholz and Kunzmann, 1993). Uranyl phosphates and silicates were used to date the formation of the granitic landscape and the kaolinitic regolith which was preserved in some depression from erosion (Dill et al., 2010). A full blown cycle of peneplanation and incision lasted from 8.4 Ma (Tortonian) onward into the early Quaternary. The youngest kaolinization, although of economic importance and exploited at Tirschenreuth by IMERYS Tableware, has no direct impact on the Mesozoic kaolinization depicted in the succeeding sections "Results" and "Discussion". The phenomenon of kaolinization during the Neogene exposed at many places can, however, be used to depict kaolinization much older and discussed in this study — Section 5.3.1 kaolin regolith (Fig. 4).

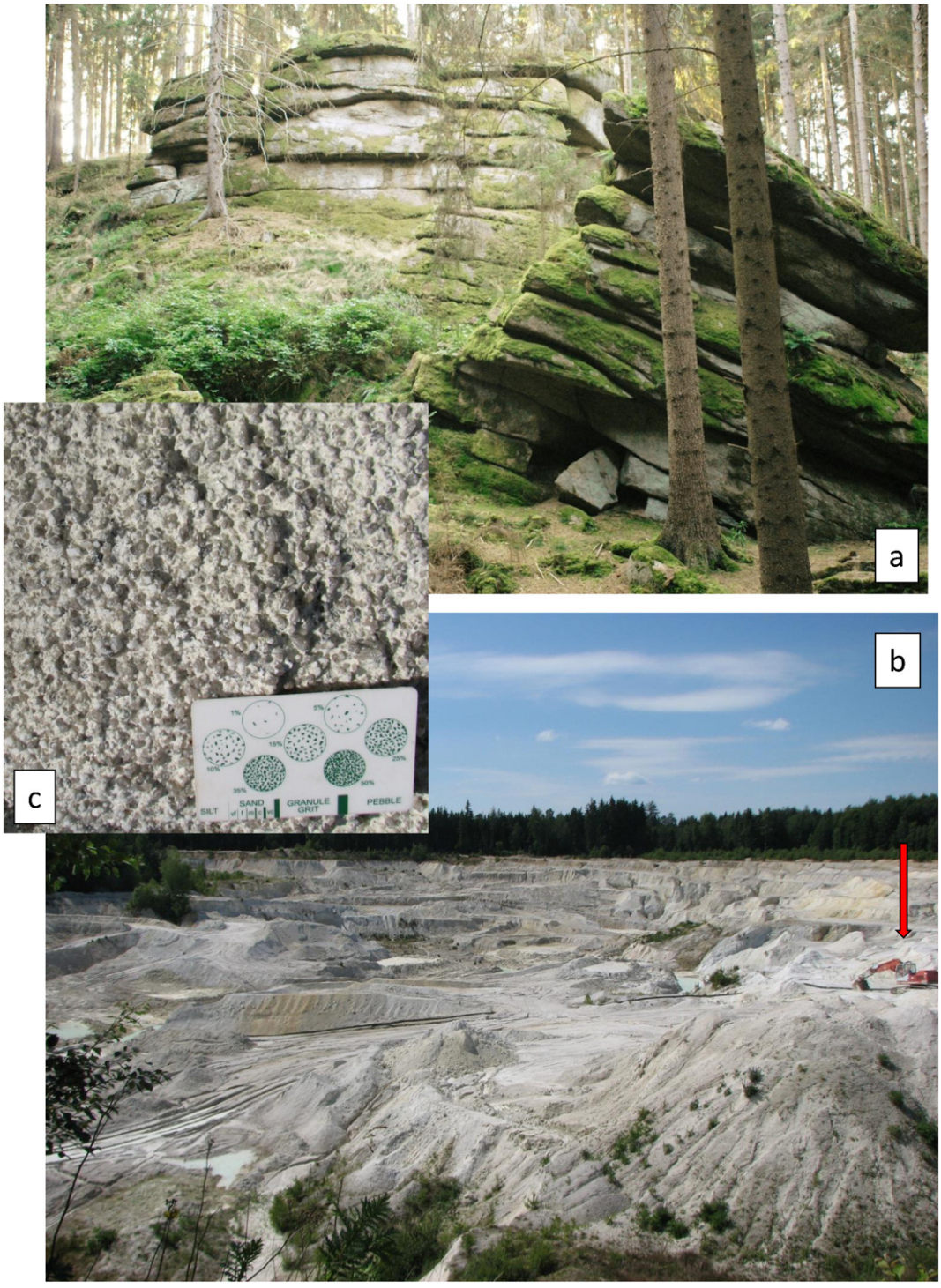

Fig. 4. The lithology, geomorphology and residual kaolin deposits around Tirschenreuth are a modern example to illustrate the kaolinization during the Permo-Triassic on top of the basement. a) Woolsacks (tors) of the Tirschenreuth granite are relics of the early Pliocene weathering or etchplain/peneplain (lower most part of the weathering front). b) Opencast mine exposing the deep-seated unzoned kaolin in the topmost parts of the Tirschenreuth granite. The vertical arrowhead points to the excavator for scale. c) Close-up view of the pervasively kaolinized Tirschenreuth granite (see grain size chart for scale). The "granitic wash" consists of quartz (dark and translucent) and white kaolin filling the interstices. The grain size scale (silt, sand, grit, and pebble) is given by dark vertical bars. In the present case the quartz grains fall into the particle range "pebble". See for comparison also the lithology of the kaolin fans at Schnaittenbach–Hirschau.

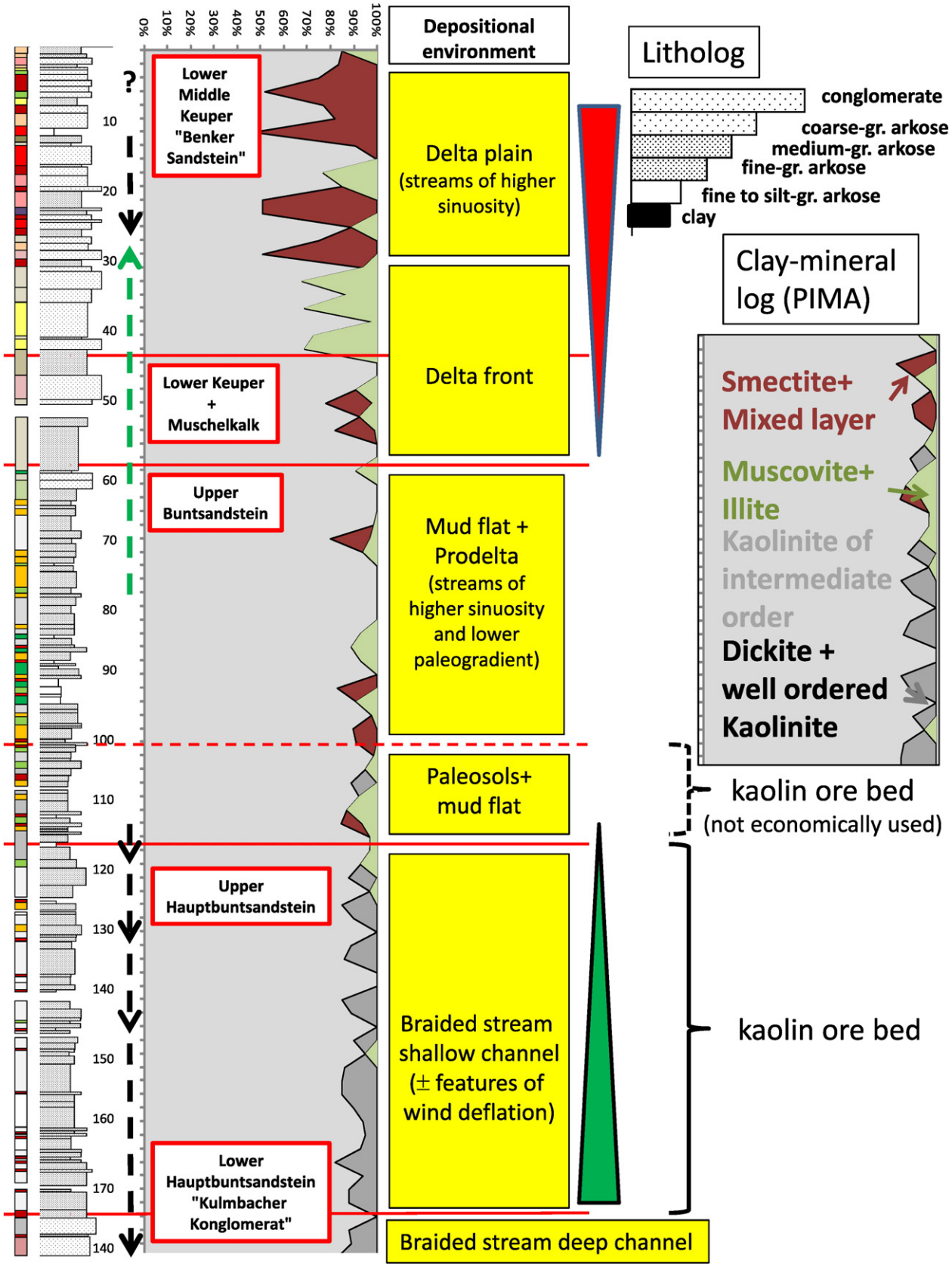

Fig. 5. Section through the Hirschau–Schnaittenbach kaolin beds. Column 1: rock color. Column 2: variable-width litholog (for legend see right-hand side). Green arrowhead = CU unit, black arrowhead = FU unit. Column 3: depth in meter. Column 4: clay mineral log based upon SWIR spectroscopy (PIMA) (for legend see right-hand side). Column 5: interpretation of the depositional environment. Term in boxes give the local names of the stratigraphic units. Green wedge = regressive part, red wedge = progressive part of the kaolin fan.

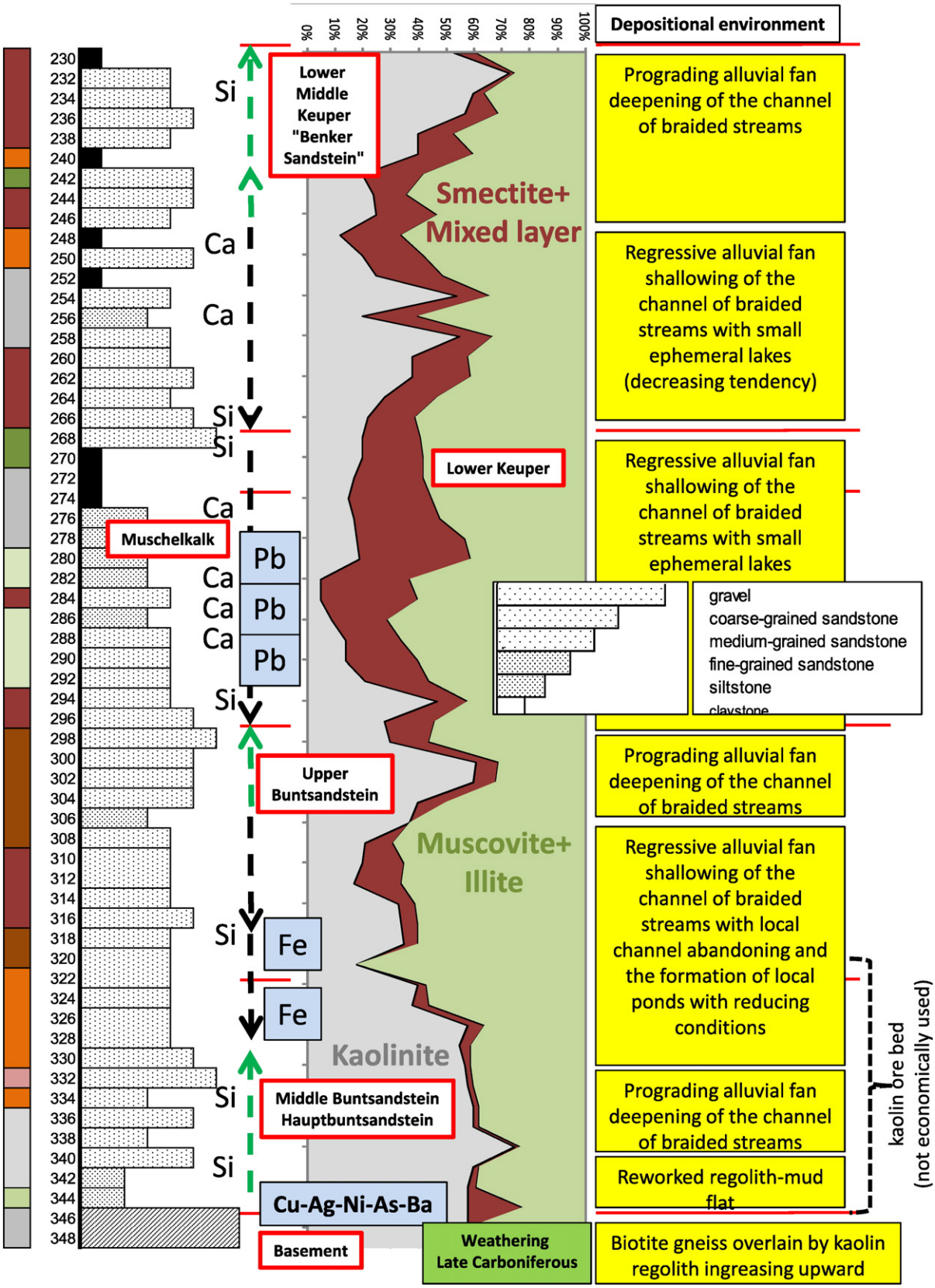

Fig. 6. DDH through the Triassic kaolin beds at Wackersdorf. Column 1: rock color. Column 2: depth in meter. Column 3: variable width litholog (for legend see right-hand side). Si = silcretes, Ca = calcretes, Pb = galena, Fe = pyrite, green arrowhead = CU unit, and black arrowhead = FU. Column 4: stratigraphy (terms in boxes give the local names of the stratigraphic units). Column 5: clay mineral log based upon XRD-based clay mineralogy. Re-calculated from Haunschild and Salger (1987). Column 6: interpretation of the depositional environment.

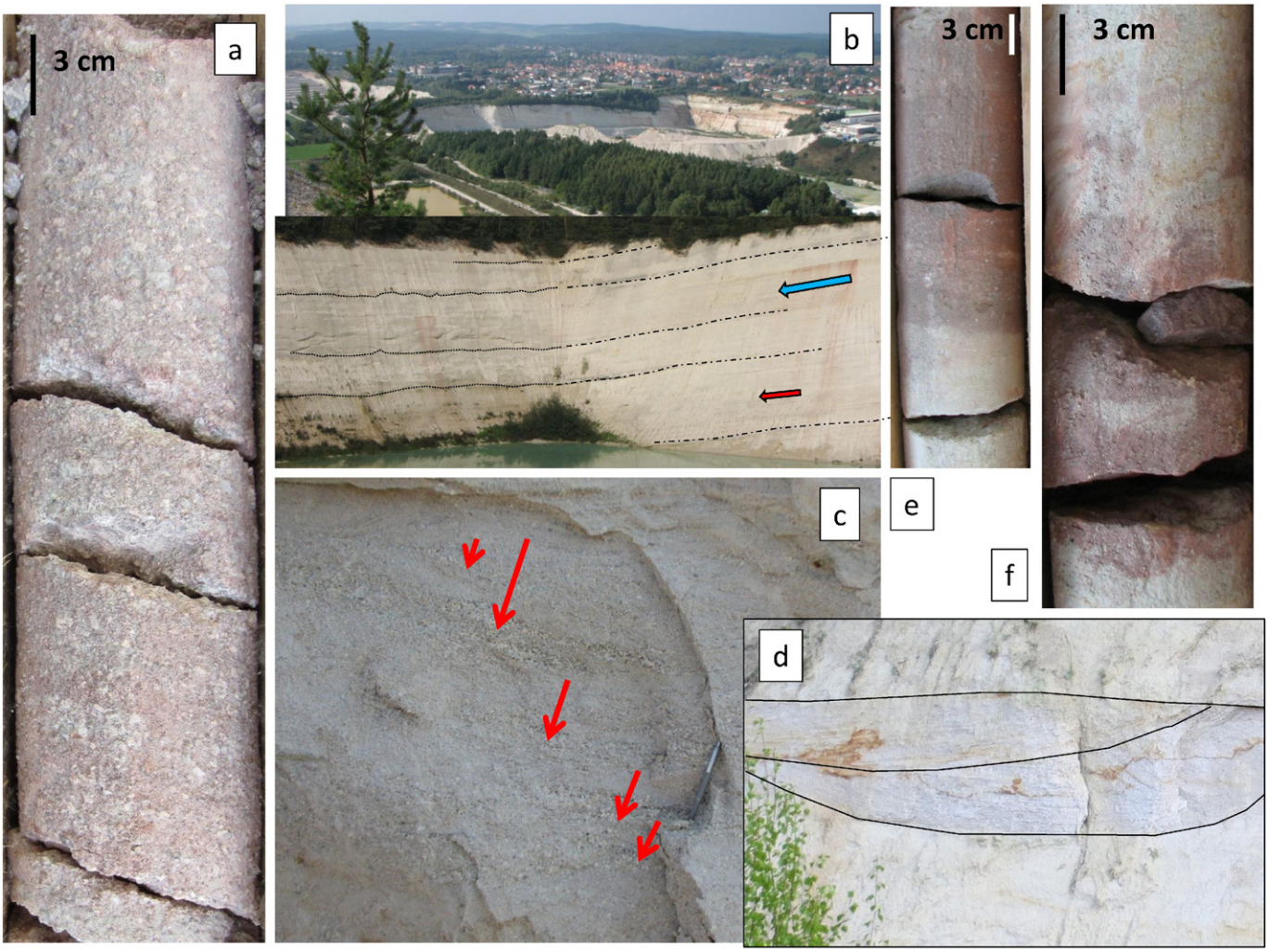

Fig. 7. Sedimentary petrography of the Hirschau–Schnaittenbach kaolin deposit. a) Footwall rocks of the kaolin ore bed at 179 m drill depth. Brown to reddish brown conglomeratic massive to vaguely bedded arkoses of the "Kulmbach Konglomerat". Depositional environment: more gravelly braided streams reflecting a more variable discharge. b) Overview of the eastern and western pits of the AKW–Kick Company in front of the town of Hirschau. The inset shows the blue pattern (paleogradient of the ore beds) and the red pattern (dip of stratification towards the NNW). The various cyclothems are marked by black lines: dash and dotted lines = longitudinal section through the depositional system, dotted lines = cross section through the depositional system downstream. Depositional environment: sandy braided streams reflecting a downstream shallowing of the channels. c) Trough cross bedding with partially kaolinized white spots of K feldspar in the western open pit (marked by red arrowheads). See biro for scale. d) Cross section through a set of channels. A younger channel incised into an older one. The bedset is truncated by the onset of the new cycle above. The arenaceous facies in this outcrop is most proximal to the source area. View facing upstream. Western open pit at Hirschau. e) Red-brown mudstone developing along an undulous contact from the gray arenaceous fine- to medium-grained sediments underneath at drill depth 114 m. Depositional environment: mud flat reflecting the most distal part of the alluvial–fluvial fan of the Buntsandstein in this area. The mottled zone in this sediments can be correlated with the silcretes elsewhere in the basin (Karneolhorizont = silcretes enriched in carnelian). f) Mottled zone displaying red-brown and gray tints above a white sandy material which is in undulous contact with the mudstone above. Depositional environment: paleosol within the upper Buntsandstein at 100 m drill depth.

4. Results

4.1. Stratigraphy and geology of the kaolin deposits

4.1.1. The Hirschau–Schnaittenbach sedimentary kaolin mining district

Mining of kaolin in the Hirschau–Schnaittenbach area takes place in the Middle Buntsandstein (Table 2). Only recently, a DDH was sunken into the sedimentary units of the Hirschau–Schnaittenbach kaolin mining district covering the entire stratigraphic sequence from the Lower Hauptbuntsandstein (Early Triassic) to the Middle to Late Triassic Keuper, represented in the uppermost section of the drill core by the "Benker Sandstein" (Fig. 5). The section has been correlated with the Triassic kaolin beds in the DDH at Wackersdorf (Figs. 2, 6). To provide a stratigraphic road map through the kaolin-bearing beds of relevance for the current study, the local stratigraphic terms are listed side-by-side with the internationally approved stratigraphic terms and age, so as to provide the reader a correlation with kaolin deposits elsewhere and show the fine-tuning of the stratigraphy of the kaolin beds in the area (Table 2). The lowermost unit hit by the drill hole is called the "Kulmbach Konglomerat" because of its conglomeratic and coarse arenaceous arkoses for the first time described near the town of Kulmbach (Figs. 5, 7a). It is a polymictic conglomerate with quartz gravel and boulders, fragments of gneisses, porphyries and granites. One distinguishing feature is the massive outward appearance of the lithology with discontinuous bedding only vaguely expressed (Fig. 7a). Locally, ventifacts can also be spotted in these conglomerates. The upper contact of the conglomerate is marked by a change in the rock color as brownish shades turned into grayish ones, typical of the ensuing kaolin ore beds (Fig. 5).

The kaolin ore beds mined at Hirschau–Schnaittenbach are restricted to the Hauptbuntsandstein, a stratigraphic unit composed of coarse- to fine-grained arkoses which were laid down in fining-upward cyclothems of different scales (Figs. 5, 7b, c, d). A pattern of stacked crossbed sets is exposed in longitudinal sections and in cross sections

in the open pit at Hirschau providing an overview of the downstream end of the paleo-drainage system (Fig. 7b).

Gravel-sized rock fragments are scarce and found only disseminated among the white arkoses, while discontinuous brown clay bands are sporadically present in the upper parts of this unit (Fig. 5). Tabular subtypes of cross bedding are less widespread than trough cross bedding in the kaolinized feldspar arkoses, forming FU sequences also on an outcrop scale (Fig. 7c). The paleogradient of the kaolin ore beds and the dip of stratification are both towards the NNW. On a larger scale, curved foreset lamellae are highlighted by partially kaolinized K feldspar being accumulated as channel lag of discrete FU units (Fig. 7c). On the south-eastern wall of the open pit or upstream wall in terms of drainage, which faces towards the source area, stacked trough-crossbed sets are exposed (Fig. 7d).

The hanging wall rocks of the kaolin ore beds belong to the Upper Buntsandstein, Muschelkalk and Keuper. The lithology of these formations shows up in the downhole plot of Fig. 5 as a coarsening-upward sequence (CU sequence) with the grain size minimum on top of the kaolin ore bed and its maximum within the "Benker Sandstein" (= sandstone). Immediately on top of the kaolin ore bed a multi-colored section stands out from the overall sedimentary petrography. The lower contact is represented by red-brown mudstone developing along an undulous contact from the gray arenaceous fine- to medium-grained sediments underneath (Fig. 7e), whereas the upper part may be described as a mottled zone displaying red-brown and gray tints above a white sandy material (Fig. 7f). Textural convulsion increases upward in this stratigraphic unit.

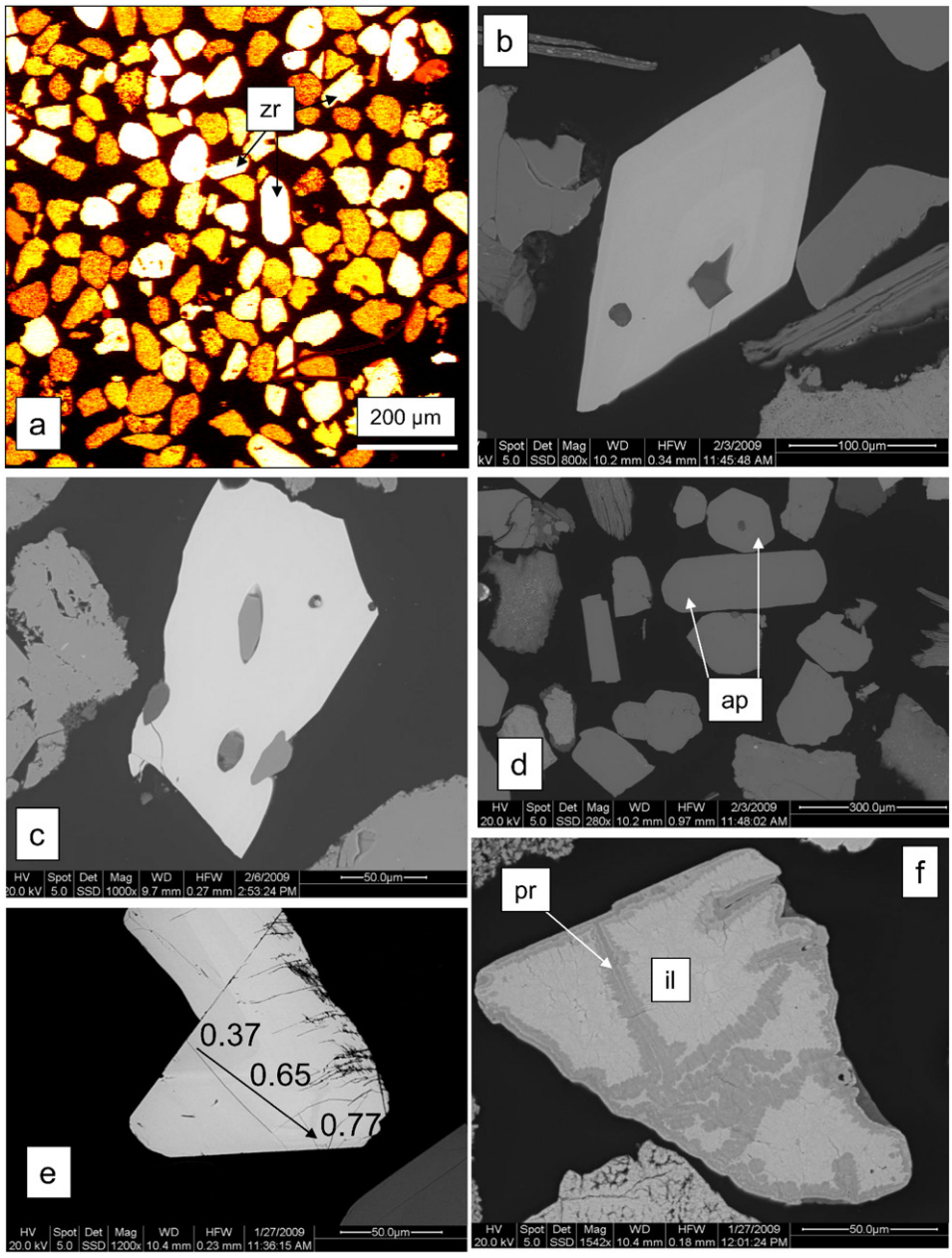

Fig. 8. Micrographs of zircon and apatite under SEM–EDX. a) Subrounded stubby crystals of zircon (zr) (type I) among rutile and ilmenite grains (false-color image). Keuper. b) Bipyramidal crystals of type II — zircon displaying a faint zonation and including quartz. Keuper. c) Corroded type III — zircon with lozenge-shaped inclusions of apatite Buntsandstein. d) Stubby prisms of apatite (type I) in Buntsandstein arkoses. e) Zoned monazite (types I and II). The Ce/Th ratios are given for three station points from the core to the rim of the monazite grain (direction of arrow). Keuper. f) Ilmenite (il) replaced along fissures by hydroxilian pseudorutile (pr). Keuper.

4.1.2. Kaolinization along the basement–foreland contact at Wackersdorf

Preliminary results of their study concerned with the Triassic sedimentary rocks penetrated by the Wackersdorf drill hole were reported by Haunschild and Salger (1987), who subdivided the entire section running from a 95-m drill depth down to the final depth of 350 m within the basement biotite gneisses (Fig. 2). Contrary to the drill hole at Hirschau–Schnaittenbach, where the kaolin ore bed is over- and underlain by sedimentary rocks which were kaolinized at a lesser degree than the ore beds, proper, at Wackersdorf, kaolinization gradually develops from strongly altered basement rocks and fades out in a sequence that is stratigraphically attributed to the Middle Keuper. The whole section measures roughly 120 m in thickness (Fig. 2). The kaolinization is most intensive in conglomeratic and arenaceous arkoses resembling those described from Hirschau–Schnaittenbach as to the stratigraphy but not with regard to the lithology and grain size variation (Figs. 5, 6). Fine-grained argillaceous sandstones, still rife with unaltered minerals of the underlying basement, mark the onset of sedimentation during the early Triassic. From this basal sediments onward the grain-size increases up (CU unit) to a drill depth of 332 m, where it is substituted by a fining-upward cycle (FU) which reaches its minimum grain size at a 306-m drill depth. This alternation of FU and CU units can be observed up to a drill depth of 298 m (Fig. 6). Higher up in the stratigraphic column, only FU and CU units can be recognized, less well expressed in the litholog than in the older stratigraphic series. Calcareous encrustations and silcretes, mainly enriched in carnelian, were encountered at various levels within the drill core. The maximum of carbonatization coincides with a considerable Pb mineralization in the Muschelkalk (Fig. 6).

4.2. Mineralogy of the kaolin deposits

At first glance, the conspicuous gray and white monotonous rock color of the kaolin-bearing sediments observed in the sections under study may be mistaken for a poor mineralogical composition, which is not the case at all. The rock-forming minerals of kaolin have been subdivided in the into three categories: (1) heavy minerals, (2) light minerals, (3) phyllosilicates.

4.2.1. Heavy minerals

4.2.1.1. Zircon. Zircon is ubiquitous in the kaolin-bearing Triassic sediments in Hirschau–Schnaittenbach and Wackersdorf. While its chemical composition and optical properties are notoriously rather constant and do not change very much, its crystal morphology is rather diverse. If well-developed faces may be recognized, the crystal form has been described using the common notation of Miller's indices (Kostov and Kostov, 1999). Kostov and Kostov (1999) published crystallographic trends and the most common crystal habits of this silicate. Zircon mainly occurs in the form of subrounded stubby crystals which were categorized as type I (Fig. 8a). Crystals of type I may be corroded and also locally infiltrated by quartz along cracks. A systematic examination of zircon morphology led to the discovery of some zircon types which do not fall into this common classification scheme put forward above. Type II may be described as bi-pyramidal with the crystal faces {211} prevailing over faces {101} (Fig. 8b). It shows a faint zonation and includes quartz. Type-III zircon is corroded and its crystal shape may only be described as stubby to rhomb-shaped. Notably, it bears inclusions of lozenge-shaped apatites (Fig. 8c).

4.2.1.2. Phosphate minerals. Judging by the morphology and intergrowth, apatite grains fall into three principal categories. Subhedral to euhedral crystals of apatite type I elongated parallel [001] are ubiquitous among the detrital components especially in the lowermost part of the drill section (Fig. 8d). In the Keuper Beds nodular apatite was spotted (type II) and aggregates of apatite are intergrown with quartz, monazite and zircon in the Buntsandstein beds (type III). While REE-bearing phosphates monazite and xenotime can be recognized in both sites under study, apatite does not play a prominent role among the heavy minerals in the kaolinized beds at Hirschau–Schnaittenbach.

Many attempts have been made to identify monazite in the heavy mineral separates or ease its distinction from zircon and xenotime (Richter et al., 2008). In the samples taken at Wackersdorf, monazite (Ce content of the sediments: 328 ppm Ce) and xenotime (Y content of the sediments: 83 ppm Y) may easily be distinguished from each other by means of SEM–EDX. In the section under study, the majority of monazite belongs to type I (monazite–(Ce–Th–La)), second most in abundance is monazite–(Ce–La–(Th)) (type II), found mainly in the basal sediments of the Buntsandstein, and only sporadically types III (monazite–(Ce–Nd)) and IV (monazite–(Ce–Th–Sm–La)) were met in the Keuper sediments. In zoned monazite s.s.s., the core used to be enriched in La (type II) and the rim enriched in Th (type I) (Fig. 8e). The highest Th contents were determined in monazite grains from sandstones of the Buntsandstein with a Th/Ce ratio of 0.87. The quantity of xenotime is by some orders of magnitude smaller than the amount of monazite (monazite: xenotime = 10: 1).

The aluminum–sulfate–phosphate minerals (APS minerals), a rather complex group of minerals deserve a particular treatment in the current study because of their significance for the determination of the physical–chemical regime of the kaolin deposits (Dill, 2001). In the Hirschau–Schnaittenbach deposit the sulfur content is extremely low and only the phosphate anion plays a role in the build-up of the APS minerals. Only the sulfate-free members of the APS solid solutions series (s.s.s.) are expected. In Wackersdorf, no member of this special phosphate s.s.s. was determined in the heavy minerals association of the kaolinized rocks, and phosphate is there exclusively bound to apatite and pyromorphite. It shall be stated that due to the low concentration it is not possible to determine the proportion of this Pb phosphate. For the first time, Störr et al. (1991) identified minerals of the crandallite s.s.s. in the kaolin of Hirschau. Their investigation was sparked by the locally elevated Pb content which could not be accounted for by a simple absorption onto kaolinite and they found plumbogummite as the host of Pb in the kaolin. Plumbogummite did not remain the only mineral of this group (Table 3). The minerals do not occur as pure end-member type but used to show up as complex s.s.s. containing the various APS minerals at variable extent, as was demonstrated by the senior author in several cases (Dill, 2001, 2003a; Dill et al., 1995a, b,c). The minerals, which can only be localized and identified by microanalytical processes, escape mechanical separation processes in the

Table 3
Correlation coefficients of phosphate and proxy elements in phosphates minerals disseminated in kaolin at Hirschau–Schnaittenbach and Wackersdorf to approximate the variation of phosphate minerals as a function of stratigraphy of kaolin-bearing Triassic stratigraphic units. Bold-faced numbers refer to correlation coefficients indicative of the phosphate minerals.

Locality	Stratigraphy	Ca	Ba	Sr	Pb	Ce	Y	V	As	Phosphate minerals
Hirschau–Schnaittenbach	Lower Middle Keuper	0.45	**0.66**	**0.83**	**0.58**	0.11	0.27	0.60	n.d.	Goyacite, gorxeixite, plumbogumite
	Lower Keuper Muschelkalk	**0.51**	0.36	0.30	**0.47**	**0.45**	**0.81**	0.51	0.36	Xenotime, crandallite, plumbogumite, monazite
	Upper Buntsandstein	0.34	**0.97**	**0.97**	−0.08	0.29	0.26	0.15	n.d.	Gorxeixite, goyacite
	Middle Buntsandstein	0.38	0.43	**0.78**	**0.57**	**0.80**	0.42	0.74	n.d.	Goyacite florencite, monazite, plumbogumite
	Concentrate of heavy minerals	−0.91	−0.35	−0.38	−0.83	**0.98**	**0.93**	**0.95**	−0.82	Monazite, xenotime
Wackersdorf	Kaolin-bearing Triassic series	**0.91**	−0.10	0.29	**0.56**	0.23	0.28	0.33	−0.03	Apatite, pyromorphite (?)

n.d. = not determined on account of low element contents which are unsuitable for statistical treatments.

processing plant (Kräuter, 2012). As the APS minerals adhere to the kaolinite plates, the crandallite s.s.s. pass only partially into the more iron oxide-containing fraction during the processing of kaolin suspensions under the influence of a magnetic field.

The kaolin–plumbogummite association is not exceptional for the Hirschau deposit. It was also found elsewhere along the western edge of the Bohemian Massif, *e.g.*, in the contact zone of the Weinsberg and Mauthausen Granites, Austria (Göd and Brandstätter, 1999). The crandallite–goyazite–gorceixite–plumbogummite association and REE phosphates vary corresponding to the stratigraphy. Unlike many other heavy minerals treated in the current study, mineralogical measures create a mineral log of the APS minerals and are not suitable for the small grain size and owing to their intimate intergrowth with kaolinite. To get an idea of the variation of APS minerals by stratigraphy the necessary steps to ensure reliable results can only be taken within the scope of chemical investigations. The correlation coefficients between phosphate and Ca, Ba, Sr, REE, Ce, La, Nd, Sm, Y, V, As, and Pb were calculated (Table 3). Arsenic and vanadium can substitute as arsenate and vanadate anion complex for phosphate in phosphate minerals under study, while the various metals mentioned above are accommodated as cations in the phosphates. Even if this approach is only a chemical approximation, it is sufficient for genetic discussions and also seen as a rough scheme to localize the APS minerals unwanted for some kaolin final products (Table 3). In the Wackersdorf area, unambiguous apatite is the only phosphate of relevance in the kaolin ($R_{P-Ca} = 0.91$). The Middle Buntsandstein (Upper Hauptbuntsandstein + uppermost part of the Lower Hauptbuntsandstein "Kulmbacher Konglomerat") shows the most complex and striking concentration of APS minerals (Table 3, Fig. 5). In Table 3 the end-members are given for the sake of clearness, and in nature, s.s.s. have to be expected, excluding xenotime and monazite which do not form part of this group but gradually disintegrate into the APS analogue florencite (Johan and Johan, 2005). A closer look at kaolin samples placing emphasis on these phosphates in kaolin yielded the following results. Cerium, yttrium and vanadium show a strongly positive correlation with phosphate, whereas the element common to APS minerals show a strikingly negative correlation. The concentration process results in an enrichment of monazite and xenotime but does not contribute to an increase of Ba-, Sr-, Ca-, Pb- and REE-bearing APS minerals. Vanadium and arsenic show strongly contrasting behavior during this step of the mineral processing. Vanadium shows the same trend as Ce and Y, whereas arsenic goes the opposite direction.

4.2.1.3. Titanium–iron minerals. Ti oxides, including rutile, anatase and ilmenite, are very widespread among the heavy minerals in the Triassic sediments and stand out by their diversity in morphology. In places, ilmenite is surrounded by a tiny rim of hydroxilian pseudorutile or replaced along fissures by pseudorutile (Fig. 8f). Single crystals of rutile are present in the heavy mineral association and found in biotite–chlorite in what is called the "sagenite" texture. Anatase occurs in well-shaped platy crystal aggregates.

4.2.1.4. Tourmaline. Tourmaline grains are rather scarce in this section and only two subtypes may be singled out among these solid solutions series. One type is close to the Fe-specialized schorl-, the other to the Mg-specialized dravite.

4.2.1.5. Sulfides and sulfates. At Hirschau–Schnaittenbach and Wackersdorf, the evolution of sulfides and phosphates strongly contrasts with each other. In Hirschau–Schnaittenbach sulfides are negligible, whereas at Wackersdorf a great variety of Pb-, Cu-, Zn-, Fe, Ni- and Ag sulfides, which were dealt with already by Dill (2010a) exists and listed below: acanthite with native silver, niccolite, bravoite, Ni marcasite, pyrite, marcasite, galena, sphalerite, chalcopyrite, and chalcocite. These sulfur-bearing minerals in the kaolinized section belong to two distinct mineral assemblages which are confined to two stratigraphic units separated from each other in space and time (Fig. 6). A Pb-dominated mineralization with galena as the prevailing sulfide was hit by the drill hole when penetrating the Muschelkalk at Wackersdorf (Fig. 6). The Cu–Ag–Ni–As–Ba mineral association lies much deeper in the stratigraphy. Its minerals are disseminated in the host rocks and straddle the "Late Variscan unconformity" at 340 m drill depth in the Wackersdorf hole. It is the only mineral association which also contains sulfate (barite) in the kaolinized beds. Hirschau has no sulfide mineralization to match those encountered at Wackersdorf, but has some chemical anomalies to correlate with (Fig. 9). In the kaolin beds at Hirschau, the silver anomaly is stratigraphically located within the Upper Buntsandstein, at a similar level as the base metal anomaly (Fig. 9). Even though, the Pb–Cu–Zn- and Ag enrichment are found in the same stratigraphic unit, there is genetic correlation between the two.

4.2.2. Light minerals

4.2.2.1. Feldspar and quartz. At Wackersdorf, plagioclase is a minor constituent and at Hirschau–Schnaittenbach within the kaolinized beds completely absent. Potassium feldspar is quite common in both sections, due to the fact that kaolinization was not to full completeness in the arkoses and left behind partially altered K feldspar mainly as channel lag deposits along foreset lamellae (Fig. 7c). The mineral grains can still be identified as a microcline under the petrographic microscope based upon the characteristic twins and described by means of XRD as a microcline intermediate (Fig. 10a, b). In addition to the microcline, in some samples from the kaolinized Keuper unit, orthoclase has been determined by means of XRD. Quartz is ubiquitous in the arkoses and conglomerates mainly as angular fragments (Fig. 7a).

4.2.2.2. Biotite and chlorite. By definition, using the specific gravity as a yardstick, biotite and chlorite should have been treated in the preceding section among the heavy minerals, but for genetic and crystallographic reasons we deviated from handling these minerals in a conventional way like that. These phyllosilicates are more closely affiliated with the light minerals than the heavy minerals. Biotite altered to chlorite and, locally, converted to muscovite is an integral part of the metamorphic basement rocks in the Wackersdorf site, where its amount gradually decreases from the basement rocks way-up into the zone of kaolinization. In the Hirschau–Schnaittenbach area, where such basement rocks are missing, it is preserved in red and brown clay interbeds within the white kaolin ore beds. Hematite and "limonite" accompany, in places, the conversion of Fe-enriched mica and chlorite as reaction products (Table 1).

4.2.2.3. Kaolinite. Kaolinite-group phyllosilicates, the sheetsilicate targeted upon during mining, are present across the entire section at Hirschau–Schnaittenbach and Wackersdorf, predominantly as polytypes kaolinite 1Md and kaolinite 1A according to the results obtained from XRD and following the classification and description used in Lanson et al. (2002), Kogure et al. (2005) and Marfil et al. (2005) (Figs. 5, 6, 10c). The samples were also investigated by MIR spectroscopy. In the graph of Fig. 10a the four characteristic OH-stretching vibrations originating from the different AlAlOH bondings are assigned the code v1–v4. The v1 through v3 vibrations result from inner surface hydroxyls whereas v4 corresponds to inner hydroxyls. Kaolinites with so called b-axis disorder (Russell and Fraser, 1994) lack the v2 stretching vibration and in the case of halloysite, both, v2 and v3, are absent. The appearance or absence or even the intensity ratio of the 3670 and 3650 cm^{-1} bands are considered reflecting the crystallinity (degree of structural order) of kaolinite (Russell and Fraser, 1994). The relative intensities do not conspicuously vary along depth or as a function of facies changes at Hirschau–Schnaittenbach. In Fig. 11 the MIR vibrations (v1, v2, v3, and v4) of a reference sample from the Hirschau–Schnaittenbach kaolin beds is calibrated to the kaolinite of low and high crystallinities of

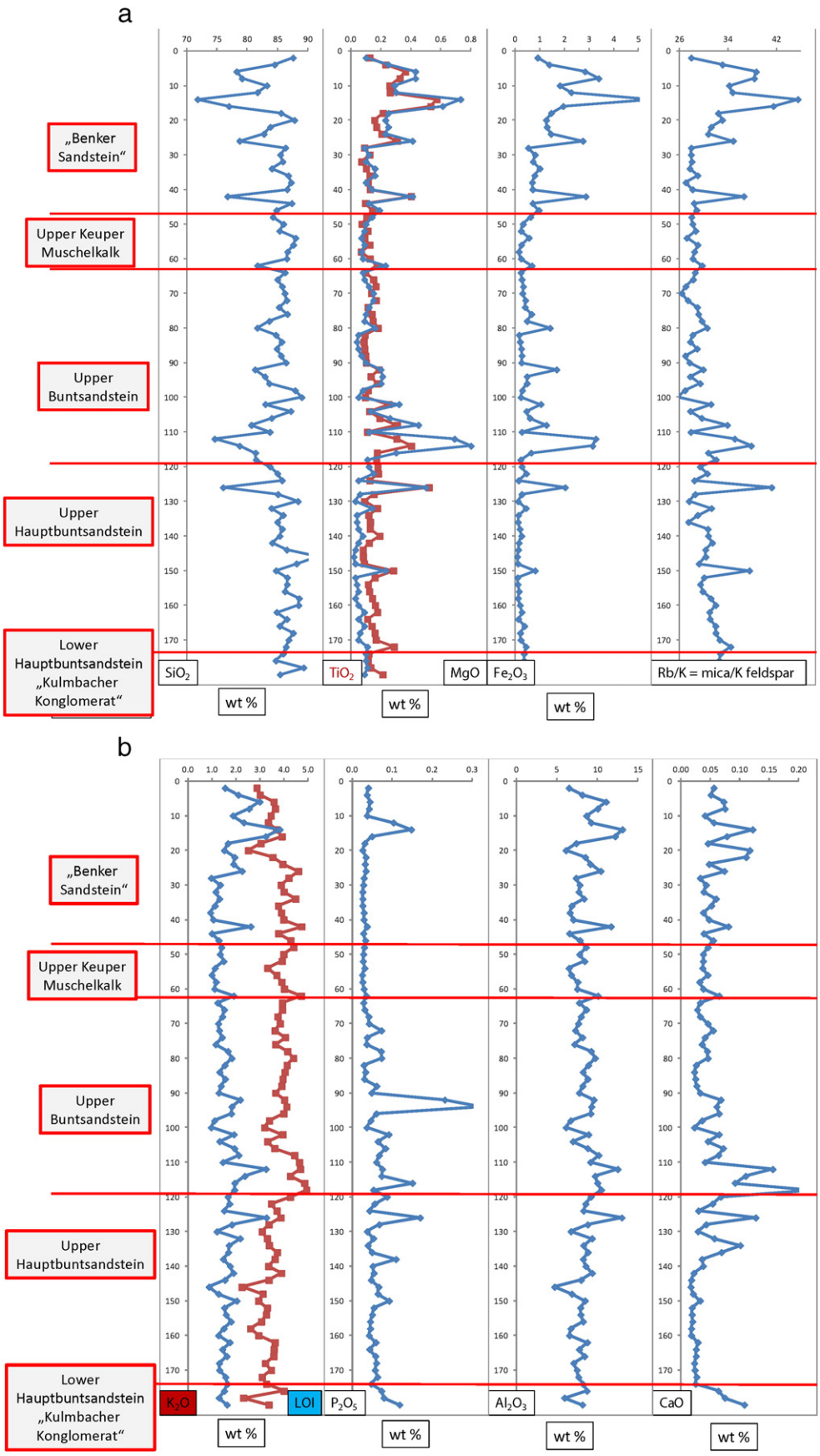

Fig. 9. Chemologs of the kaolinized beds of the Hirschau drill hole. a) SiO_2, TiO_2, MgO, Fe_2O_3, and Rb/K = K mica/K feldspar. b) K_2O, LOI, P_2O_5, Al_2O_3, and CaO. c) REE, Pb, Cu, Zn, Zr, and Ag.

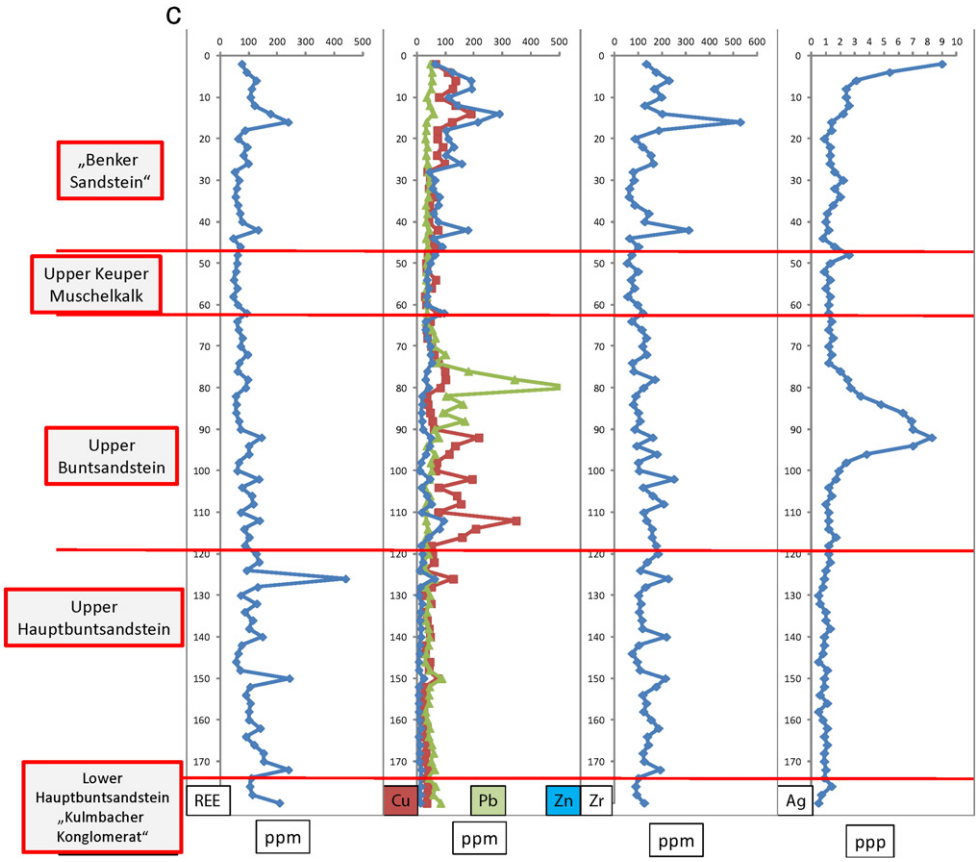

Fig. 9 (*continued*).

the Pleystein pegmatite (SW Germany). Accordingly, the low intensity of the band at 3670 cm^{-1} indicates a lesser degree of crystallinity compared to the high-crystallinity kaolinite from Pleystein. It may be referred to as a kaolinite of "intermediate crystallinity".

To achieve the goal to characterize the kaolin already in the field and to get a full-blown clay mineral log in a reasonable time span, short-wave infra-red (SWIR) spectrometry, commonly known as PIMA-based survey (PIMA = portable infrared mineral analyzer), has been used following the proposals for its handling published, *e.g.*, by Adams and Gasparini (1970), Dill (2003b), Günzler and Gremlich (2003), and Bowitz and Ehling (2008). Fig. 10b displays a SWIR spectrum for the Hirschau–Schnaittenbach kaolinite. It shows the diagnostic components in its lattice and their response to the SWIR radiation. In the downhole plot of Fig. 5 an enhancement of the crystallinity can be deduced from the SWIR/PIMA-log. Dickite found in the PIMA log as a minor constituent could not be proved unequivocally by means of XRD in the laboratory. The PIMA graphs were, however, compared with reference samples of dickite to substantiate the appearance of dickite in the clay mineral log and assure its presence for further discussion.

4.2.2.4. Muscovite–illite. The micaceous phyllosilicates are common constituents of both study areas (Figs. 5, 6). Judging by the XRD analyses they are assigned to the muscovite 3 T and muscovite 2 M1 group of micaceous phyllosilicates.

4.2.2.5. Smectite plus mixed-layer. The 10 Å phyllosilicates mentioned in the previous paragraph are rarely present as pure mica, but frequently form part of mixed-layers together with smectite. In Figs. 5 and 6 those micaceous mixed-layers dominated by smectite and smectite *sensu stricto* are plotted together as a function of stratigraphy and their environment of formation because for the whole section it was difficult to draw a comprehensive picture for this group of phyllosilicates. Salger (1958, 1979) has already given particular attention to this mixed-layer phyllosilicates in the Triassic sediments. He used in his subdivision of smectite-group minerals and its mixed-layers in the kaolinized Triassic beds the basal spacing at 12 Å, 14 Å and 18 Å. Mixed-layers with a widely spaced reflection in the interval 12–14 Å is common to the upper kaolin beds in the Hirschau drill hole, corresponding to a mixed-layer of $illite_{80}$–$smectite_{20}$.

4.3. Chemistry of the kaolin deposits

The tripartite set of chemologs gives on overview of the variation of major (Fig. 9a, b) and trace elements (Fig. 9c) with depth. Additionally, in Fig. 9a the rubidium/potassium ratio is on display to assess the variation of the K mica relative to K feldspar with depth. In Fig. 9b an increase of the phosphate content is shown towards older series which does not correlate with the calcium contents. In the chemologs of the trace element contents anomalies exist in the Upper Hauptbuntsandstein, the kaolin beds, proper, for REE (Fig. 9c). Base metals are enriched in the Upper Buntsandstein but their contents fall short of what might be expected for Pb-, Zn- and Cu mineralization. The silver contents are conspicuously enriched in the same stratigraphic interval, yet with no correlation with any of the base metals. Zirconium was accumulated in the "Benker Sandstein" and shows some "spikes" in the Upper Hauptbuntsandstein (Fig. 9c).

5. Discussion

5.1. Depositional environment and kaolinization

The kaolinization has attracted the attention of various geoscientists for genetic reasons and those dealing with this type of deposit after the Second World War are mentioned in this discussion. Those, however,

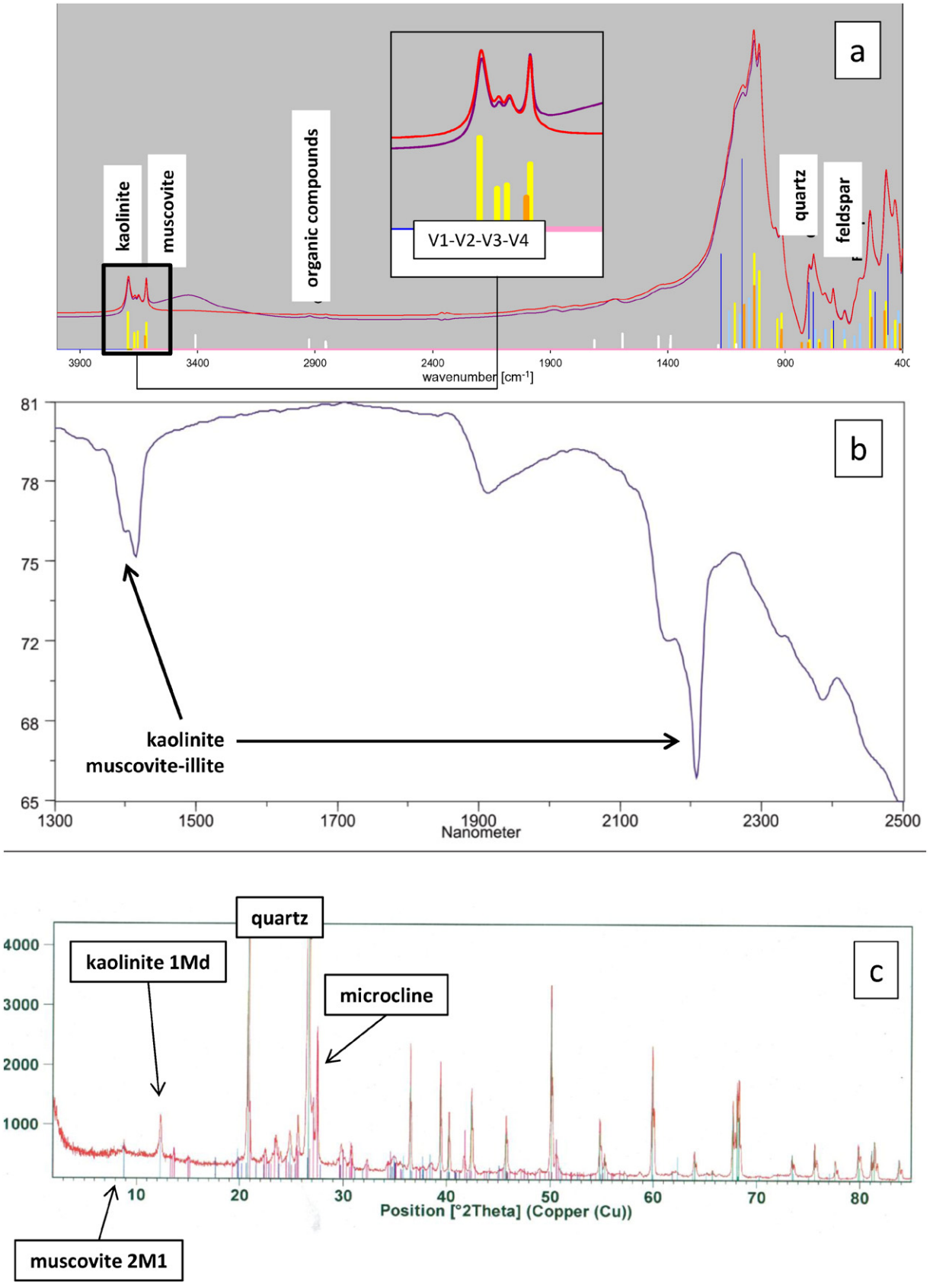

Fig. 10. Reference spectra of kaolin from Hirschau–Schnaittenbach using different methods. a) MIR spectrum (mode/y-axis relative absorbance). The inset displays a close-up view of the four characteristic OH-stretching vibrations indicative of kaolinite. The red graph gives the MIR spectrum of the dry sample. b) SWIR spectrum (mode/y- axis percentage of reflectance) basis for the downhole plot (Fig. 5). c) XRD spectrum (mode/y-axis counts).

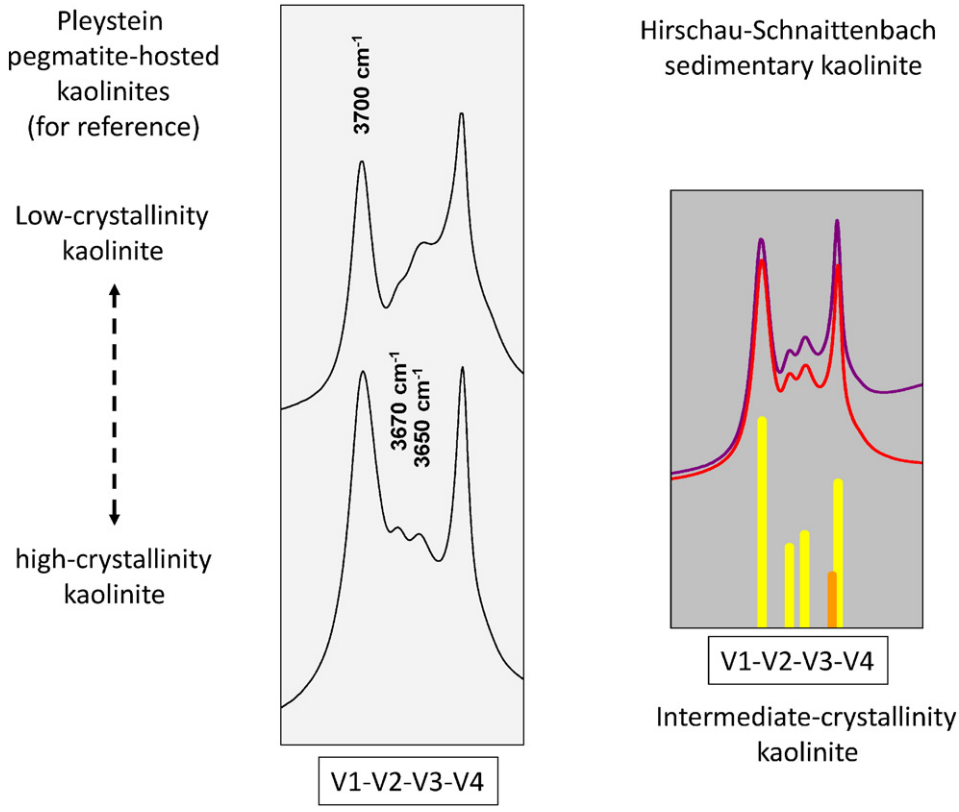

Fig. 11. Intensities of MIR vibrations (v1, v2, v3, and v4) of the Hirschau–Schnaittenbach kaolinite calibrated to the kaolinite of low and high crystallinities of the Pleystein pegmatite (SW Germany).

studying the deposits or the surrounding Triassic rocks prior or during to the Second World War have been mentioned by Salger (1958) who was the first after the war to study these deposits. This historical reference was completed later by Köster (1974) during his study of the "Oberpfälzer Kaolinlagerstätten". The pre-war history of stratigraphical investigations mainly by local geologists was given by Tillmann (1940). The researchers are mentioned here in chronological order and the reader being interested in a more historical approach is referred to the above authors: Rösler (1902; cited by Steinlein, 1939), Rasel (1909; cited by Steinlein, 1939), Stahl (1912), Heim (1936), Knetsch (1929), and Steinlein (1939).

The environment analysis conducted in the current study is not an end in itself but the platform to work upon and understand the succeeding sections dealing with the hydraulic and hydrographic conditions and the physical-regime regime controlling the kaolinization (Figs. 5, 6, 7, 12). An overview of the principal parameters and features to interpret the different lithofacies types of these terrigeneous clastic depositional systems are given in the textbooks of Galloway and Hobday (1996), Miall (1999) and Selley (2000). In the Hirschau–Schnaittenbach area a cyclic but steady shallowing of the basin took place during the Hauptbuntsandstein, whereas from the Upper Buntsandstein upward a consequent coarsening upward can be recognized and interpreted with a renewed uplift in the hinterland (Fig. 5). The regressive ("green wedge") and the progressive fans ("red wedge") are separated from each other by a depositional environment, where bed load deposition ran almost down to nil and suspended load became the prevailing process. The commercial part of the kaolin beds is located within a braided river drainage system ("green wedge"), typical of abundant sediment supply, high stream and channel gradients accompanied by fast and intensive variations of water discharge (Fig. 5) (Miall, 1977, 1992, 1994, 1996; Bristow, 1993; Bridge and Mackey, 1993; Bridge, 2003). Miall (1977) elaborated various vertical facies models which he categorized and named after reference drainage systems in Northern America. The shallowing of the channel system described in the current study resembles most closely the transition from the "Saskatchewan-Type" into the "Platte-Type" drainage system, two sandy braided-river-drainage systems. The "Kulmbach Konglomerat" reached at final depth in the drill hole attests to a transition from sandy braided rivers into gravelly braided rivers ("Scott Type"), which formed at a more proximal position within the alluvial fan system (Fig. 12). Ventifacts were encountered among the gravel in this stratigraphic unit. These special morphological types bear witness of a vast plain that allowed for deflation and unimpeded access of the wind to shape and polish the cobbles and pebbles. The onset of the formation of the mudflat is marked in the chemolog by an increase in Ti, Fe, and Ca, which stand for some kind of a paleosol. The coarsening upward sequence which gradually evolves from this mudflat or prodelta has all hallmarks of an alluvial delta, with a delta front and delta plain terminating this sequence. This is also accentuated by the variation of the Zr spikes (Fig. 9c). In the kaolin beds of the Buntsandstein, the spikes are less intensive, of almost equal size with a relative minimum in the prodelta environment. The REE contents follow suit with the zirconium contents which mirror the variation of zircon, in particular, and the detrital input, in general.

The depositional environment at Wackersdorf, albeit of the same age, strongly contrasts with the Hirschau–Schnaittenbach area (Figs. 5, 6). A kaolin regolith gradually develops from a biotite-gneiss, and the evolution of the braided-river drainage system reflects a prograding alluvial fan indicative of strong uplift in the hinterland. Unlike at Hirschau–Schnaittenbach, several relapses marked by FU units occur. They are indicative of a cessation of uplift or even regression with a shallowing of the channel and with local channel abandoning resulting in the formation of local ponds which favored reducing conditions. A change from a more prograding into a more regressive alluvial fan took place during the Muschelkalk and Keuper, while the channels of braided streams were shallowing and small ephemeral lakes came into existence (Fig. 6). Calcareous and siliceous encrustations furnish

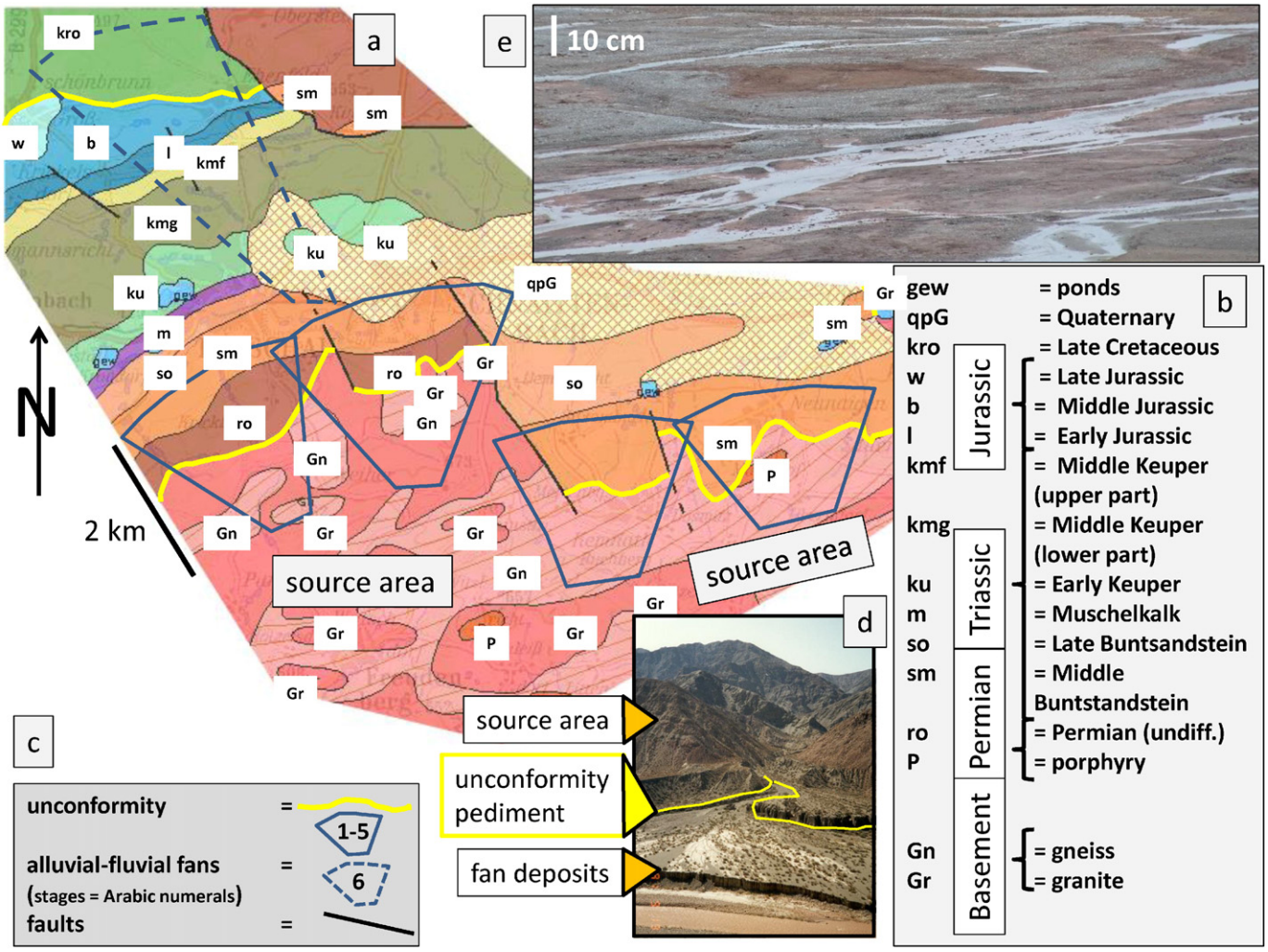

Fig. 12. Geological setting and alluvial–fluvial kaolin fan deposits. a) Geological map of the study area (geological basis: BIS = Geo Information System of Bavaria). The map shows the alluvial–fluvial kaolin fan deposits (blue bold-faced line) amalgamating to a fan apron or bajada fan during the Early Triassic Middle Buntsandstein (sm) and spreading across the Late Variscan unconformity. In the western part, Permian platform sediments encroached upon basement gneisses and granites, and in the eastern part, the kaolin beds directly overly the basement rocks. Another kaolin fan evolved during the Late Cretaceous, eroding into the exhumed kaolin beds at Hirschau–Schnaittenbach (blue stippled line). b) Geological legend for the stratigraphic units and lithologies on display in the geological map. c) Key to structures shown in the geological map. d) Alluvial fan with braided streams flowing out of the uplifted source rock area in the hinterland. Example: Pleistocene fan of the San Juan Valley, Argentina. e) Holocene sandy braided stream deposits from the Liefdefjord on Svalbard, Norway.

clear evidence of groundwater and pedological driven duricrust formation during this period of time.

A comparison of both depositional environments reveals that in both settings, kaolinization is confined to alluvial fans with predominantly sandy arenaceous braided-river-drainage systems. A consequent evolution of the alluvial fan system from a strong rate of uplift in the hinterland to a lower rate of uplift was more favorable for the kaolinization than an intensive *in-situ* kaolinization accompanied by a frequent back-and-fro of the transport system.

Moderately ordered to well-ordered kaolinite and even dickite developed in environments of deposition, displaying a consequent evolution from a regressive alluvial fan at the beginning which is the stage of concentration ("green wedge") of kaolin to a prograding alluvial fan which stands for the stage of preservation ("red wedge") of the kaolin deposits, providing a seal to the reservoir. Periods of tectonic quiescence, marked by an enlargement of mud flats in Hirschau–Schnaittenbach and ephemeral small lakes and ponds were detrimental to the kaolinization and more favorable for the formation of smectite and smectite–illite mixed layers rather than kaolinite-group minerals due to the low water level below ground.

5.2. Source area and kaolinization

To decipher the source area where the kaolin-bearing sediments came from forces us to take a closer look at the detrital or allochthonous heavy minerals disseminated in the kaolin beds. In the Hirschau–Schnaittenbach area rutile, tourmaline, monazite, xenotime, zircon, magnetite, and biotite are assigned to this group of minerals, and at Wackersdorf, zircon and apatite accompanied by a little garnet, tourmaline, monazite, xenotime, rutile, titaniferous magnetite, biotite (altered), and ilmenite belong to the weathering residues. Owing to their abundance and morphological diversity, zircon and phosphate rank first among the heavy minerals suitable for provenance analysis. Zircon grains are ideally suited for a crystallographic discrimination, due to the strong resistance of zircon against weathering as well as its extreme variability in crystal morphology that has sparked several petrological studies aimed at correlating crystal morphology with the environment of formation in the source rocks (Pupin, 1980; Benisek and Finger, 1993; Bingen et al., 2001). The detrital heavy minerals in the kaolin beds under study most efficacious as marker minerals are zircon and apatite that point to Precambrian H–T metamorphic rocks of the

Moldanubian Zone, which in Wackersdorf are represented by the biotite gneisses just underneath the Triassic beds, and to the Upper Carboniferous and Permian felsic to intermediate volcanic rocks, which were recorded from water wells undercutting the kaolin beds and shown in the geological map of Fig. 12 (Haunschild, 1979). Both source lithologies were exposed in the catchment areas of the alluvial–fluvial drainage systems during deposition of the Early Triassic kaolin beds when the roof of the granites made of Precambrian gneisses was still intact and the Upper Carboniferous and Permian felsic to intermediate subvolcanic rocks were of more widespread occurrence than today (Fig. 12). The present-day landscape shows large areas underlain by granites and gneisses, but little porphyries at the outcrop and gives a picture of the Mesozoic and Cenozoic uplift (Fig. 12). These provenance analyses have implications as to the concentration of REE in kaolin which is more REE-prone when derived from gneisses (Fig. 9c).

Although kaolin can originate from a wide range of parent lithologies, running the gamut from ultrabasic igneous rocks through felsic rocks, parent material abundant in feldspar has without any doubt an edge over feldspar-poor rocks (Köster, 1974; Dill et al., 1995c; Harben and Kužvart, 1997; Lorenz and Gwosdz, 1997; Ruiz Cruz and Reyes, 1998; Schroeder and Shiflet, 2000; Lanson et al., 2002; Marfil et al., 2005; Alü Sayin, 2007). In the present situation, heavy-mineral based constraints on the source rocks, reveal that both kaolin deposits are situated close the source rock, with Wackersdorf at a more proximal position (apatite "in"), resting unconformably on kaolinized crystalline basement rocks and Hirschau–Schnaittenbach at a more distal position (apatite "out"), measuring approximately 5 to 10 km between source and depocenter.

5.3. Kaolinization, kaolin alteration and the physical–chemical regime

Kaolinization in the Mesozoic sedimentary rocks and the Precambrian source or parent rocks is a complex multi-stage process. In addition to the strong control exerted by the facies of deposition, chemical and physical processes that are discussed in the succeeding sub-chapters for each stage of kaolinization play a vital role. The entire process of kaolinization has been subdivided into six stages for the kaolin fans under study: (1) weathering of the parent rock (residual kaolin), (2) transport and deposition (synsedimentary to early-diagenetic kaolin), (3) synsedimentary to late-diagenetic alteration of kaolin, (4) late diagenetic alteration of kaolin, (5) epigenetic alteration of kaolinization, and (6) exhumation and redeposition of kaolin. Like the sedimentary facies, physical–chemical processes can be classified either as constructive, preserving or destroying.

5.3.1. Weathering of the parent rock and the formation of a kaolin regolith (Stage 1)

Kaolinization affected the crystalline basement rocks at Wackersdorf prior to the deposition of the early Triassic kaolin-bearing sedimentary rocks. It is truly supergene with the facies-diagnostic minerals kaolinite, illite/muscovite and apatite. Based upon these minerals the physical–chemical regime during kaolinization can be calculated (Fig. 13a). The Eh–pH diagram in Fig. 13a depicts the physical–chemical regime of the phosphate mineralization at 25 °C during kaolinization of the crystalline bedrock, using the dissolved species as $\log_{aCa} = -4$, and $\log_{aHPO4} = -3$. The pH during development of the residual kaolin was greater than pH = 6. This physical–chemical calculations are consistent with the presence of kaolinite and muscovite as well as K feldspar, all of which are associated with phosphate and assumed to develop according to the reactions below (Fig. 13b).

$$2\ \text{K feldspar} + 2H^+ + 9H_2O \Rightarrow \text{kaolinite} + 4H_4SiO_4 + 2K^+$$

$$\text{illite} + 4.2H_2O + 0.8H^+ \Rightarrow K^+ + 0.25Mg^{2+} + 0.3Al(OH)_4^- + 1.5H_4SiO_4 + \text{kaolinite}$$

The Eh–pH diagram portraying the stability fields of the newly formed phyllosilicates kaolinite and illite at 25 °C, using the dissolved species as $\log_{aAl} = -4$, $\log_{aSiO2} = -4$, and $\log_{aK} = -4$ reveals an overlap with the stability fields of Ca phosphate. The residual kaolinization took place under mildly acidic to mildly alkaline conditions (pH 6 to 8) typical of an alternating dry and wet climatic regime known from the savannah of present-day Central Africa (Twidale, 2002). The weathering process is constructive in terms of the emplacement of a residual kaolin deposit.

5.3.2. Reworking and transport — synsedimentary to early-diagenetic kaolin (Stage 2)

At Wackersdorf, reworking and transport of kaolin during the early Triassic Buntsandstein took place under physical–chemical conditions not at variance with what has been described in the previous section (Figs. 6, 13a, b). It was mainly a mechanical process under almost identical conditions. In the depositional environments illustrated in Fig. 6, the presence of silcretes ("carnelian") stands out. Calculations performed in a similar way for these silica compounds but not shown explicitly in a diagram reveal the concentration of dissolved species of silica to increase in meteoric fluids while the pH values of the fluids rise. At 25 °C and using the dissolved species as $\log_{aSiO2} = -3$, below pH 11 solid phases such as quartz or its fine-grained modification chalcedony may exist. The pH of the meteoric fluids gradually moved towards higher values and the stability field of smectite and its mixed-layers with illite expanded (Fig. 6). Pyrite, locally, present in the kaolin is indicative of reducing conditions.

The litholog in Fig. 5 displays a totally different picture for the Hirschau–Schnaittenbach area during the early Triassic Buntsandstein. Kaolinite is abundant, mica is rare and apatite is absent in these sediments. The mineral assemblage differs from that of Wackersdorf and cannot be interpreted as climatic-controlled, because over a distance of less than 25 km no climate change may be expected. The Hirschau–Schnaittenbach kaolin beds rest upon Permian sediments known to be abundant in kaolinite, mica and apatite (Salger, 1979). What is the reason for the mineralogical difference between the different types of kaolin fan deposits? The unconformity between the crystalline basement rocks and the Buntsandstein siliciclastic rocks at Wackersdorf and the boundary between Permian and Triassic sediments at Hirschau–Schnaittenbach mark the onset of a reducing and an oxidizing alluvial–fluvial kaolin fan, respectively. At Wackersdorf, the back-and-fro during fan evolution discussed in Section 5.1 provoked the formation and the preservation of local reducing zones enriched in base metal sulfides. By contrast, the consequent drainage system at Hirschau–Schnaittenbach favored the generation of an overall oxidizing alluvial–fluvial fan with physical–chemical conditions detrimental to apatite but favorable for kaolinite and APS minerals (Fig. 13c). The pH dropped significantly down to a pH in the range from 1.5 to 6, in these oxidized kaolin fan deposits. Under this very low pH range, APS minerals and kaolinite are very stable. Nevertheless, slightly increasing pH values in the meteoric fluids even allow for the preservation of K feldspar and muscovite in so-called lag deposits (Fig. 7c). The red arrowhead plotted in Fig. 7c denote in the cross-bedsets a slight downward-increase of the grain-size, which according to Selley (2000) correlates with a variation of porosity and permeability. In trough-shaped cross-bedding, foreset sands curve down into silty toesets resulting in a decrease of permeability. *Vice versa*, tabular–planar cross-bedding leads to the opposite grain-size and permeability changes.

Contrary to this, the "window" of the SiO_2 activity is very narrow, with the $\log_{SiO2(aq)}$ oscillating around −4 (Fig. 7c). Therefore, neither zeolite, nor pyrophyllite or gibbsite have been reported from the Hirschau–Schnaittenbach kaolin. By contrast, apatite, which is very vulnerable to acidic meteoric fluids, was eradicated to completeness under these strongly acidic conditions. Kaolinization was most efficacious in the oxidizing alluvial fan under strongly acidic conditions and accounts

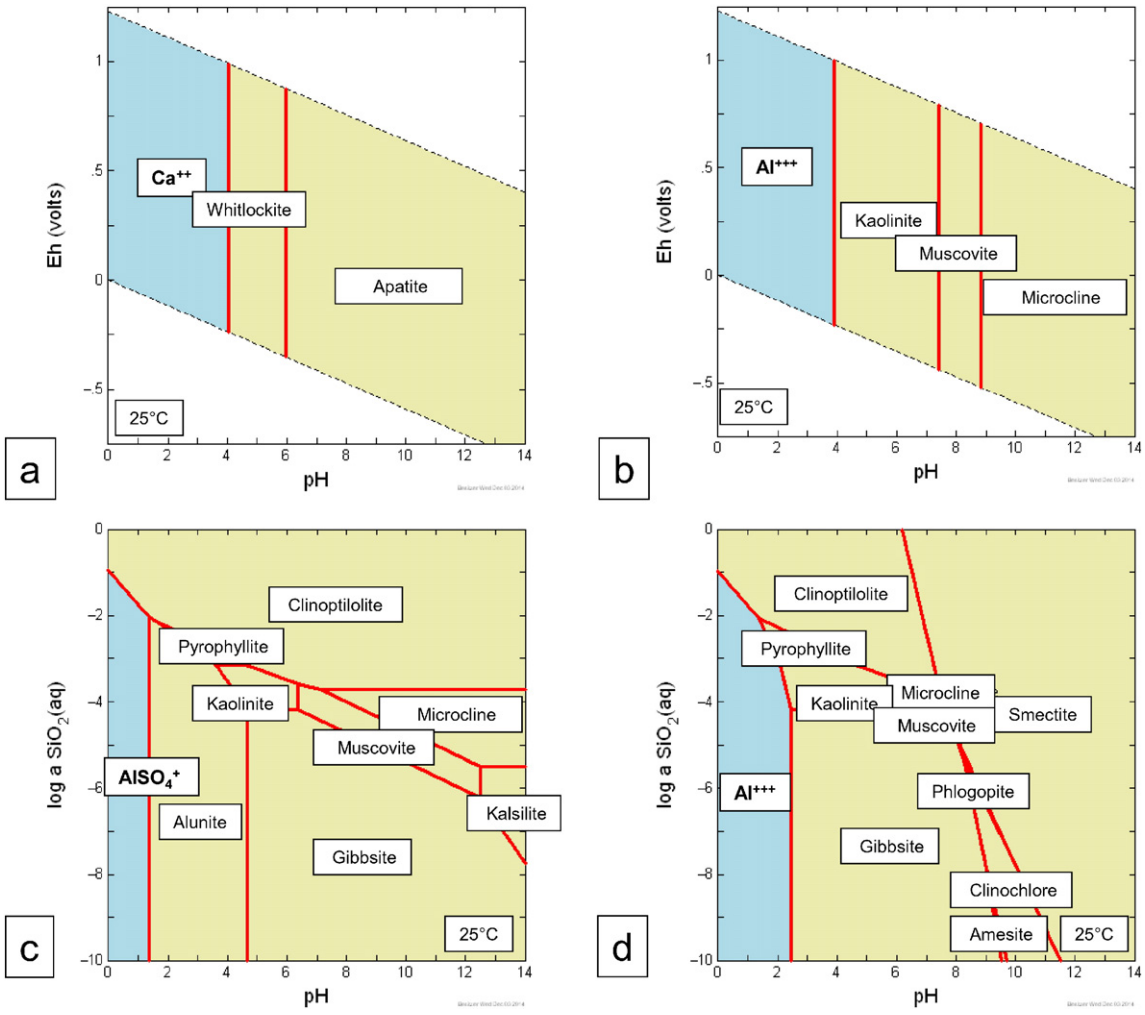

Fig. 13. Diagrams of sedimentary the kaolinite facies. Assumed concentrations of dissolved species are given below in mol/l. a) Eh–pH diagram to show the phosphate mineralization at 25 °C during kaolinization of the crystalline bedrock using the dissolved species as $\log_{aCa} = -4$, $\log_{aHPO4} = -3$. b) Eh–pH diagram to show the newly formed phyllosilicates kaolinite and illite at 25 °C during kaolinization of the crystalline bedrock using the dissolved species as $\log_{aAl} = -4$, $\log_{aSiO2} = -4$, and $\log_{aK} = -4$. c) $\text{Log}_{aSiO2\ (aq)}$–pH diagram to show the kaolinite–APS mineralization at 25 °C. The dissolved species are given as $\log_{aK} = -3$, $\log_{aMg} = -3$. d) $\text{Log}_{aSiO2\ (aq)}$–pH diagram to show the smectitization of kaolinite mineralization at 25 °C using the dissolved species as $\log_{aK} = -3$ and $\log_{aSO4} = -3$.

for the concentration of kaolinite at Hirschau–Schnaittenbach relative to Wackersdorf from the chemical point of view.

The delta-like sedimentation in Hirschau–Schnaittenbach during the Keuper sealed off the kaolin beds and protected them from erosion. Kaolinization was of synsedimentary to early-diagenetic origin in both alluvial–fluvial fans. The aeolian impact on the sediments (see Section 5.1) shaping the cobbles and pebbles document that the kaolinization in this oxidized kaolin fan took place at very shallow depth or in other words under near-ambient conditions, that is additional proof for the Eh value above 0 (volt). The physical–chemical conditions and depositional system were constructive and preserving, working in the same direction and thereby accounting for the emplacement of these kaolin fan deposits in this region.

5.3.3. Synsedimentary to early-diagenetic alteration of kaolin (Stage 3)

Vertically upward in the stratigraphic column, the amount of smectite and smectite–illite mixed layers tend to increase at the expense of kaolinite in both sections under study (Figs. 5, 6). The computation illustrated by the x–y plot of Fig. 13d suggests a continuous and steady increase in alkalinity of the meteoric fluids at Hirschau–Schnaittenbach whereas at Wackersdorf the amount of smectite increases discontinuously. This change in the clay mineral log marks a chemical change driven firstly by the climate, which became more arid, and secondly by the hydrography of each kaolin fan.

The pH of the solutions accountable for this mineralogical change fluctuates within the interval 7 to 9. The pH value may even increase during the Muschelkalk as calcretes precipitated and small ephemeral lakes came into being and expanded in size towards younger series. Locally, a reducing regime is attested by the presence of base metal sulfides, prevalently galena at Wackersdorf (Fig. 6). At Hirschau–Schnaittenbach only a chemical anomaly within the upper Buntsandstein hallmarks this event (Fig. 9c). The mineralization under consideration is neither timebound, nor stratabound or stratiform. It is facies-controlled by the mud flats (Fig. 5) and by the shallowing-upward trend of the channel system, eventually draining into ephemeral lakes at Wackersdorf (Fig. 6). The origin of this Pb accumulation has been investigated by Dill and Berner (2014) and illustrated in a transect through a stratigraphically equivalent lithology more basinward than the kaolin fan deposits, where kaolinized sandstones and arkoses are still widespread, yet no longer of economic importance for kaolin and only attracted the attention of exploration geologists for the sandstone-hosted non-sulfidic Pb deposits, as they were described among others by Bjørlykke and Sangster (1981), Melchiorre et al. (2001), Dill et al. (2008a, b), Szczerba and Sawłowicz (2009), and Pirajno et al. (2010) (Figs. 1, 14). The environment of deposition hosting

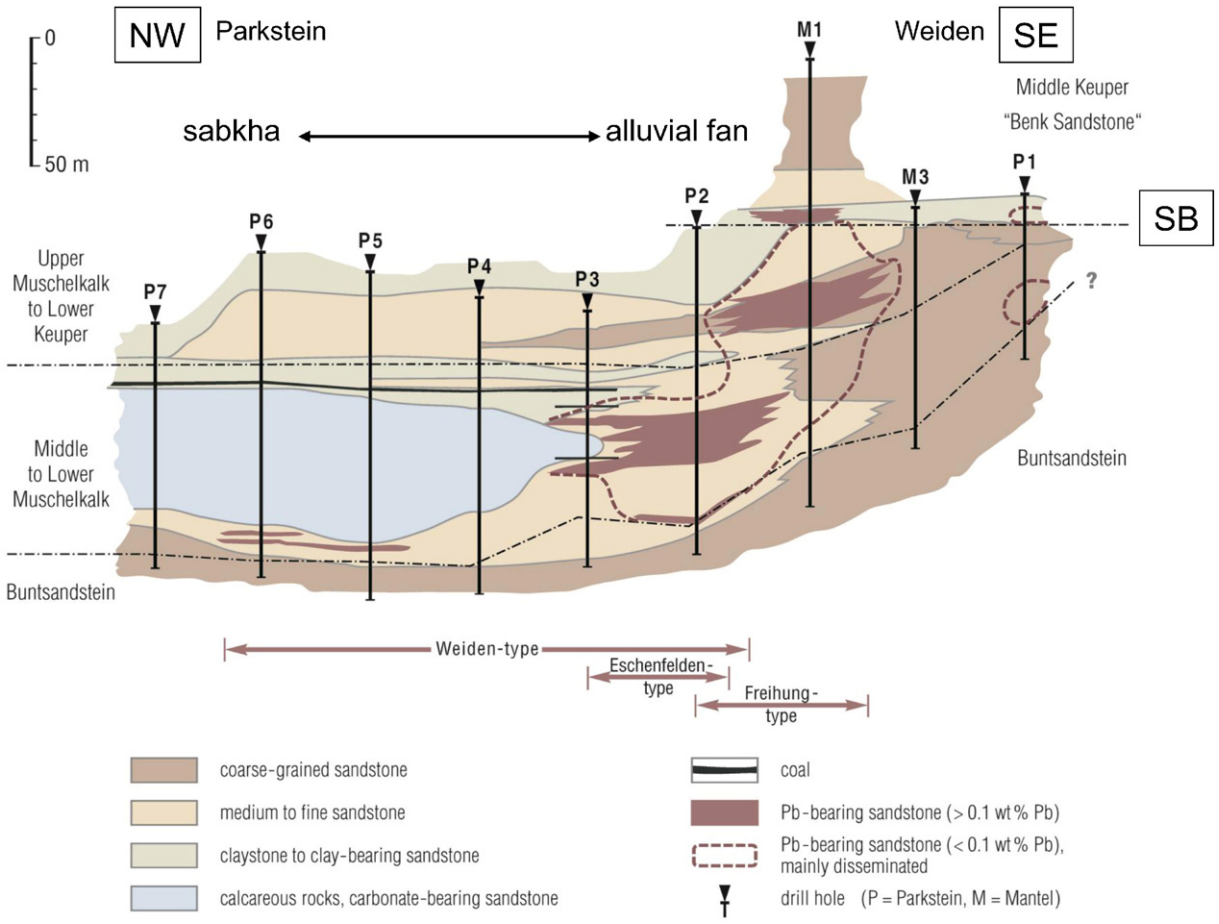

Fig. 14. Faciesbound Pb-dominated base metal concentration in Triassic kaolin sandstones and arkose in the Parkstein region (Dill and Berner, 2014). The cross section shows a Freihung-Type Pb structurebound mineralization developing from an Eschenfelden-Type flexure-related mineralization which was superimposed on a faciesbound Weiden-Type mineralization. For localization of the sites see Fig. 1. The faciesbound Pb mineralization formed more basinward from the Hirschau–Schnaittenbach and Wackersdorf kaolin fans.

non-sulfidic Pb deposits more basinward has been described in terms of a sabkha, applying a flood recharge model with an increase of concentration and downward percolation of the brines under the force of gravity towards the basin center as described from reference types by Kendall (1992), Tucker (2001), and Warren (2010). At the basin margin, this ore facies is represented by impure calcareous rocks and kaolinized arkoses with sulfidic Pb mineralization in the reduced kaolin fan (Fig. 6), whereas in the oxidized fan deposits (Fig. 5) only anomalously high base metal contents can be recognized.

While the calcretes and smectite-group phyllosilicates came into existence during early diagenesis, the base metals followed during a later stage of diagenesis. Smectitization of kaolin and the base metal mineralization took place during the late Muschelkalk and the Keuper (Benker Sandstone).

5.3.4. Late diagenetic alteration of kaolin (Stage 4)

In the lowermost part of the kaolin beds of Hirschau–Schnaittenbach minor amounts of dickite and well-crystallized kaolinite were identified with a downward-increasing trend (Fig. 5). Dickite is known to have a wide stability field in terms of diagenesis-metamorphism, covering the range from the boundary between early to late diagenesis to the high anchizone, which means, when being translated into temperature of formation, a T interval of 100 °C to 300 °C (Dill et al., 1997; Ruiz Cruz and Reyes, 1998; Merriman and Peacor, 1999; Lanson et al., 2002). McAulay et al. (1994) suggests the kaolinite–dickite conversion to be a dissolution–reprecipitation process. The hypothesis of a depth- or burial-related replacement of kaolinite by dickite has to be discarded in case of the Hirschau kaolin deposits, because the critical interval for the kaolinite's conversion into dickite between 2500 m and 5000 m burial depth has never been reached in the marginal part of this epicontinental basin (Lanson et al., 2002). Other parameters than a rising temperature on burial have played a more prominent role in the formation of dickite. According to Lanson et al. (2002) early precipitation of kaolinite is related to flushing by meteoric waters — see above. Subsequent diagenetic kaolinite–dickite transformation resulted from the invasion of acidic fluids of organic origin. The kaolinite–dickite conversion is kinetically controlled.

5.3.5. Epigenetic alteration of kaolin (Stage 5)

In the reducing alluvial–fluvial kaolin fan at Wackersdorf sulfide–arsenide minerals are disseminated above and underneath the unconformity between the basement and the Triassic kaolin beds (Fig. 6). In the oxidizing alluvial–fluvial kaolin fan at Hirschau–Schnaittenbach, a chemical anomaly of silver in the Upper Buntsandstein series is the only expression of this mineralization (Fig. 9c). The faciesbound Pb ore bodies of stage 3 increase in size and in ore grade towards the basin center along with the paleogradient. While dipping basinward they cross the stratigraphic boundaries towards older units (Figs. 5, 6, 14).

The Ag mineralization of stage 5, however, provides an equally reverse situation, while crossing basinward the stratigraphic boundaries towards younger units (Fig. 9c). The geohydraulic plane controlling this Ag-bearing mineralization cuts through Triassic beds which were tilted by post-Triassic faulting. It is a paleoaquifer that runs subparallel to the early Cretaceous unconformity. Gilg (2000) claimed a late Early Cretaceous kaolinization age for the Early Triassic sandstone-hosted

deposits at Hirschau–Schnaittenbach, which can definitely be excluded by geological and mineralogical reasons discussed in this paper. One of the reviewers (M. Störr) recommended a more detailed discussion of the age of formation, with special reference to the hypothesis of an Early Cretaceous kaolinization, which is discarded in this study (Gilg, 2000). One of the first comprehensive studies devoted to the clay mineral associations in the Lower Triassic Series (Buntsandstein) was performed by Becher (1965), who unraveled the lateral facies change from the basin edge to the basin center. The entire Buntsandstein in the Schnaittenbach–Hirschau area belongs to a kaolinite province which is substituted more basinward by an allevardite province covering the stratigraphic sequence of the lower and middle Buntsandstein, whereas the upper Buntsandstein is represented by an illite province. Both clay mineral provinces still contain kaolinite yet with a decreasing trend towards the basin center. More basinward the allevardite province is replaced by a chlorite province extending into the lowermost parts of the upper Buntsandstein. The illite province is replaced more basinward by a corrensite province. There is no vertical change of the kaolinite distribution reported in this study; it is strictly controlled by the paleogeographic changes in an epicontinental marine–continental basin. Kaolinite can be encountered within the Middle Buntsandstein together with illite underneath marine Middle Triassic Muschelkalk beds more than 100 km away from the basin edge (Dill, 1976). If the kaolinization had taken place during the Early Cretaceous the overlying Muschelkalk and Keuper beds should have been affected much more than the underlying Buntsandstein, reflecting a downward-decreasing rather than a downward-increasing trend for stratigraphic issues (see Table 2). There are several deep drill holes sunken into this Late Paleozoic–Mesozoic sedimentary basin fill by the former Geological Survey of Bavaria, showing more conspicuously, a decreasing kaolinization from the basin edge to the basin center, underneath a pile of marine and continental sediments with little or no kaolinization underneath the Early Cretaceous peneplain/unconformity. Along with these remarkable changes in the clay mineral association, a variation of the Pb–Cu–Zn content may be observed within the terrigeneous sediments (Dill and Berner, 2014). This mineralogical and geological barrier is also shown in the reference hole at Wackersdorf, where sediments more than 150 m thick lack any kaolinization rest on top of the kaolin beds and separate the Early Cretaceous weathering front from the Lower Triassic Bunter Series (Fig. 2).

Oxygen isotopes may be useful to determine the temperature of formation during kaolinization applicable to climatic assumptions but is not helpful as a fingerprint for the age of formation as demonstrated for the kaolinization in Great Britain, Brazil, South Africa, and Egypt (Sheppard, 1977; Giral-Kacmarcík et al., 1998; Harris et al., 1999; Parnell et al., 2000; John et al., 2012; Baioumy, 2013). The small epigenetic unconformity-related mineralization was a unique effect of probably early Cretaceous age, restricted to the metals mentioned above, but without any impact on the nature of the clay mineral assemblage.

5.3.6. Exhumation of the Triassic fan deposit and redeposition of kaolin (Stage 6)

The last sedimentary event that affected exclusively the oxidized kaolin fan deposits was detrimental to the Hirschau–Schnaittenbach kaolin deposits, but did not provoke their denudation to full completeness (Fig. 12). During the Late Cretaceous, the kaolin deposits resting unconformably on the late Paleozoic platform sediments and on the crystalline basement rocks were considerably uplifted and brought into the reaches of erosion. As a consequence, another arenaceous kaolin fan-delta complex evolved to the North of Hirschau–Schnaittenbach (Fig. 12). The Senonian and Turonian kaolinitic clays at Ehenfelden, are kaolin redeposited from the Early Triassic arkoses of Hirschau–Schnaittenbach (Köster, 1974) (Fig. 12). This reworking of kaolin was corroborated by trace element analysis and furnish further evidence for the Triassic age of kaolinization in the kaolin fan deposits discussed in previous sections.

5.4. Kaolin fan deposits and the current classification schemes of kaolin deposits

Kaolin fan deposits are representative of a unique environment of deposition, forming a separate entity among the sedimentary kaolin deposits. The compilation of industrial minerals by Harben and Kužvart (1997), *e.g.*, did not address this mode of formation and proposes a grouping into four types: (1) weathering, (2) hydrothermal, (3) solfatara-type, and (4) mixed type. Lorenz and Gwosdz (1997) subdivided kaolin deposits into three genetic groups: (1) residual kaolin deposits/primary, (2) hydrothermal kaolin deposits/primary, and (3) sedimentary kaolin and kaolinitic clays/secondary. By all accounts, weathering forms part of the sedimentary processes and as such belongs to the sedimentary petrology, even if it includes a lot of issues and processes also known from pedology, hydrology and climatology (Tucker, 2001). Therefore, Dill (2010b) splitted the kaolin deposits during his first-order classification in the "Chessboard classification scheme of mineral deposits" according to their host rocks into two basic types, magmatic and sedimentary deposits. As kaolinite is not stable under low-grade regional metamorphic conditions, no equivalent compartment exists for metamorphic kaolin deposits. The magmatic part was further subdivided into five groups: (1) allophane in volcaniclastics (53 CD–53 H), (2) halloysite in skarn deposits distal to low sulfidation-type deposits (54b CD), (3) halloysite in shallow high- and low sulfidation-type deposits (54a CD), (4) nacrite–dickite–kaolinite–halloysite in shallow high- and low sulfidation-type deposits (55a CD), and (5) kaolinite in vein–greisen–pipes of granitic rocks (55b D). In the five-fold classification scheme of sedimentary kaolin deposits, the current type of kaolin fan deposits is addressed in category 55a H and 55a J: (1) allophane in andosols (53 H), (2) halloysite in paleosols (54a H), (3) residual kaolinite (55a H), (4) kaolinite reworked into siliciclastic rocks and of diagenetic origin (55a J), and (5) kaolinitic interseam sediments in coal (55a N).

Kaolin fan deposits are truly sedimentary in origin and bridge the gap between residual kaolin deposits/primary and sedimentary kaolin deposits/secondary, as shown above by Lorenz and Gwosdz (1997). The term secondary is misleading, because kaolin formation takes place in the kaolin-fan deposits in a primary way, in the strict sense. It formed *in-situ* from rock-forming minerals of the crystalline basement rocks at the fan apex and *in-situ* from rock-forming minerals of the arkoses along the fan wedge. The term secondary can only be used for intraformational reworking during the evolution of the kaolin fan deposits (Fig. 5, see above the kaolin ore beds *sensu stricto*) or during epigenetic reworking after the unroofing of the entire kaolin-fan deposits, as it is discussed in stage 6. Both processes are characterized sedimentologically by a change from bed load to suspended load deposition and in terms of applied economic geology accompanied either by an upgrade of kaolin or its downgrading into kaolinitic clays.

The present study is a fine-tuning of this existing classification scheme. It is also aimed at a launch pad for further investigations into terrigeneous depositional environments of kaolin situated more basinward, *e.g.*, high-sinuosity drainage systems (meandering streams) or anastomosing drainage systems as to their impact on the accumulation, preservation or destruction of kaolin deposits. The latter are only scarcely represented in the study areas in SE Germany. They were only being touched and studied in a section of Fig. 5 in what was denoted there as mud flat and prodelta. Streams of higher sinuosity and lower paleogradient (anastomosing) are expected but less well expressed than the braided-stream environment upstream. The same can be applied to what was called the delta plain deposits, where the lithology of the FU sequence is interpreted in terms of streams of higher sinuosity.

5.5. Kaolin fan deposits and sedimentary kaolin deposits related in space and time

How does this type of kaolin fan deposits fit in time and space into the existing scheme of kaolin deposits, of which only a few can be taken reference here? Kaolin quarried at Podbořany, Czech Republic, immediately overlies the late Variscan unconformity in the form of a paleoregolith. Its kaolin is found redeposited within arkoses and conglomerates of Late Carboniferous age (Kužvart, 1968; Wilson and Jiranek, 1995). The kaolin from the Podbořany region occurs in feldspathic sandstone of the Líně Formation (Fig. 1). Climatic conditions favorable for the formation of kaolin prevailed in the Westphalian and Stephanian and also substantiate the most favorable climatic period for the formation of the regolith in the reduced kaolin fan deposits at Wackersdorf (Fig. 1).

As far as the paleofacies is concerned the fluvial drainage system under study resembles the kaolin prospect in the Yenyening Lake District, W Australia, spreading across a pediment (Salama, 1997). The Australian reference kaolin is accumulated much closer to the regolith of the bedrock and the syn-diagenetic alteration moderate compared to the kaolin in the study area. Large kaolin districts like the Jari and Campim districts in Brazil or Weipa, Australia are part of a lateritization process and not comparable with the class under study (Dill, 2010a). The kaolinite-bearing Huber Formation of east Georgia, USA, was formed from metamorphic- and igneous derived silicate minerals and *in situ* weathering products from the Piedmont. These kaolin-bearing sediments were transported by rivers to Late Cretaceous and Early Tertiary inter-deltaic, estuaries, and back-barrier island localities (Schroeder and Shiflet, 2000). The settling of suspended river sediments as they encountered estuarine waters occurred by flocculation and by suspension-feeding organisms (*i.e.*, formation of fecal pellets). The depocenter, the way of transport and the mediating effect of organism strongly contrasts with what has been recorded from the kaolin fan deposits in SE Germany. The second reworking at Hirschau–Schnaittenbach during the Late Cretaceous evolved in a way quite similar to what has been encountered at Czerwona Woda and Zebrzydowa, Poland, in a deltaic environment (Dill et al., 2008b; Galos, 2010) (Fig. 12). The complex processes in prograding and regressive fan deposits under varying redox conditions and closely linked to the kaolin regolith are certainly more widespread in sedimentary kaolin deposits elsewhere in the world, but their value for exploration and exploitation has obviously not been recognized to the extent they deserve. In the closing section, the characteristic items are summarized, and the genetic and economic conclusions are drawn (Table 1).

6. Genetic and economic conclusions

The following genetic and economic conclusions can be drawn from the current study of the oxidized and reduced kaolin fan deposits:

- Oxidized fans are characterized by drainage systems with a lower paleogradient than their reduced analogues and they provide more favorable conditions for an efficacious kaolinization.
- The hydrography in reduced fans is marked by alternating periods of deposition and erosion at a high-frequency caused by a discontinuous rate of uplift in the hinterland and resulting in a lower preservation potential for kaolin deposits in the fan system.
- Lithological variation in the source area is not decisive to the formation of the initial residual kaolin which lies at a more proximal position in the reduced fan, relative to the fan apex than in the oxidized fan. The oxidized fan can evolve at a more distal position on non- or low-kaolinized parent rocks.
- Given a tropical climate with alternating wet and dry seasons the geoacidometers (marker minerals for low pH) are ore guides to a high potential for kaolin.
- Reduced kaolin fans are prone to base metal sulfides and arsenides which can be deleterious for the kaolin raw material and exclude its use for special final products.
- Oxidized kaolin fans may be prone to dickitization (the clear nature is not yet fully understood).
- Oxidized kaolin fan deposits may undergo intraformational or synsedimentary reworking into proximal kaolin deposits, which can also be tested as economic provided the frequency of sedimentary facies variation is not higher than that of the source deposit. In both fan types, kaolin is bed load- rather than suspended-load controlled.
- Reduced kaolin fan deposits grade into equivalent lithologies more basinward that are of economic importance for kaolin but an exploration target for the sandstone-hosted non-sulfidic Pb deposits. Elevated Pb contents in reduced kaolin fan deposits may turn out to be deleterious to the run-off mine kaolin, whereas oxidized kaolin fan deposits are less prone for base metal accumulation, which is an asset for the run-off mine kaolin raw material.
- The PIMA device has also proven in this type of deposit to be an efficacious tool for the identification and quantification of clay minerals in sedimentary kaolin deposits (quality control).

Acknowledgement

Chemical analyses were carried out in the laboratory of the Federal Institute for Geosciences and Natural Resources at Hannover by F. Korte. The preparation of samples and SEM analyses were performed by D. Klosa. D. Weck has carried out the XRD analyses. H. Hein performed the IR analyses, N. Schleuning determined the CEC. We thank Amberger Kaolinwerke (AKW)–Kick GmbH & Co. KG (Quarzwerke Frechen) for providing access to their open pits and for allowing us to examine and sample their exploration drill hole. We thank especially the mine geologist of AKW, A. Braatz. We extend our gratitude also to IMERYS Tableware, Tirschenreuth, engineer G. Grießhammer. M. Scharnhorst took the photograph of the braided streams on Svalbard, Norway. We thank one anonymous reviewer for the helpful comments made to our first draft and also M. Stoerr for his review for *Ore Geology Reviews*. We extend our gratitude also to F. Pirajno chief editor of *Ore Geology Reviews* for his editorial handling of our paper.

References

Abeysinghe, P.B., Fetherston, J.M., 1999. Kaolin in Western Australia. West Aust. Geol. Surv. Miner. Resour. Bull. 19, 1–141.
Adams, J.A.S., Gasparini, P., 1970. Gamma-ray Spectrometry of Rocks. Elsevier, Amsterdam (307 pp.).
Aigner, T., Bachmann, G.H., 1992. Sequence-stratigraphic framework of the German Triassic. Sediment. Geol. 80, 115–135.
Alü Sayin, S., 2007. Origin of kaolin deposits: evidence from the Hisarcik (Emet-Kütahya) deposits, Western Turkey. Turk. J. Earth Sci. 16, 77–96.
Baioumy, H., 2013. Hydrogen and oxygen isotopic compositions of sedimentary kaolin deposits, Egypt: paleoclimatic implications. Appl. Geochem. 29, 182–188.
Becher, A., 1965. Eine Tonmineralabfolge vom Beckenrand zum Beckeninneren im Buntsandstein Nordost-Bayerns. Beitr. Mineral. Petrogr. 11, 586–613.
Benisek, A., Finger, F., 1993. Factors controlling the development of prism faces in granite zircons: a microprobe study. Contrib. Mineral. Petrol. 114, 441–451.
Bingen, B., Davis, W.J., Austrheim, H., 2001. Zircon U–Pb geochronology in the Bergen arc eclogites and their Proterozoic protoliths, and implications for the pre-Scandian evolution of the Caledonides in western Norway. Geol. Soc. Am. Bull. 113, 640–649.
Bjørlykke, A., Sangster, D.F., 1981. An overview of sandstone lead deposits and their relation to red-bed copper and carbonate-hosted lead–zinc deposits. Economic Geology, 75th Anniversary Volumepp. 178–213.
Bowitz, J., Ehling, A., 2008. Non-destructive infrared analysis: a method for provenance analysis of sandstones. Environ. Geol. 56, 623–630.
Bridge, J.S., 2003. Rivers and Floodplains. Whiley-Blackwell, Oxford (504 pp.).
Bridge, J.S., Mackey, S.D., 1993. A revised alluvial stratigraphy model. In: Marzo, M., Puidefabregas, C. (Eds.), Alluvial SedimentationSpecial Publication 17. International Association of Sedimentologists. Blackwell Scientific Publications, Oxford, pp. 319–337.
Bristow, C.M., 1977. A review of the evidence for the origin of kaolin deposits in SW England. Proceedings of the 8th International Kaolin Symposium and Meeting on Alunite, Madrid-Rome, September 1977, pp. 7–16.

Bristow, C.S., 1993. Sedimentary structures exposed in bar tops in the Brahmaputra River, Bangladesh. In: Best, J.B., Bristow, C.S. (Eds.), Braided RiversSpecial Publication 75. Geological Society Publishing House, Bath, pp. 277–289.
Bruke, A., 2006. Half full or half empty? Filling North America's kaolin demand. Ind. Miner. 2006, 28–34.
Clark, R.,.N., 1999. Spectroscopy of rocks and minerals, and principles of spectroscopy. In: Rencz, A.N. (Ed.), Manual of Remote Sensing. John Wiley & Sons, New York, pp. 3–58.
Cravero, F., Dominguez, E., Iglesias, C., 2001. Genesis and applications of the Cerro Rubio kaolin deposit, Patagonia (Argentina). Appl. Clay Miner. 18, 157–172.
Dill, H.G., 1976. Untersuchungen in der Permo-Trias und im Buntsandstein nordöstlich Bayreuth auf Blatt Weidenberg. Geol. Bl. Nordost-Bayern 26, 235–244.
Dill, H.G., 2001. The geology of aluminum phosphates and sulfates of the alunite supergroup: a review. Earth-Sci. Rev. 53, 35–93.
Dill, H.G., 2003a. A comparative study of APS minerals of the Pacific rim fold belts—with special reference to South American argillaceous deposits. J. S. Am. Earth Sci. 16, 301–320.
Dill, H.G., 2003b. PIMA — supported exploration of industrial minerals in Mongolia and Thailand. Erzmetall 56, 20–28.
Dill, H.G., 2010a. Authigenic heavy minerals a clue to unravel supergene and hypogene alteration of marine and continental sediments of Triassic to Cretaceous age (SE Germany). Sediment. Geol. 228, 61–76.
Dill, H.G., 2010b. The "chessboard" classification scheme of mineral deposits: mineralogy and geology from aluminum to zirconium. Earth-Sci. Rev. 100, 1–420.
Dill, H.G., Berner, Z.A., 2014. Sedimentological and structural processes operative along a metalliferous catena from sandstone-hosted to unconformity-related Pb–Cu–Zn deposit in an epicontinental basin, SE Germany. Ore Geol. Rev. 63, 91–114.
Dill, H.G., Klosa, D., 2011. Heavy-mineral-based provenance analysis of Mesozoic continental-marine sediments at the western edge of the Bohemian Massif, SE Germany: with special reference to Fe–Ti minerals and the crystal morphology of heavy minerals. Int. J. Earth Sci. 100, 1497–1513.
Dill, H.G., Fricke, A., Henning, K.-H., Theune, C.H., 1995a. An aluminum–phosphate mineralization from the hypogene La Vanguardia kaolin deposit (Chile). Clay Miner. 30, 249–256.
Dill, H.G., Fricke, A., Henning, K.-H., Gebert, H., 1995b. An APS mineralization in the kaolin deposit Desa Toraget from northern Sulawesi/Indonesia. J. SE Asian Earth Sci. 11, 289–293.
Dill, H.G., Fricke, A., Henning, K.-H., 1995c. The origin of Ba- and REE-bearing aluminum–phosphate–sulfate minerals from the Lohrheim kaolinitic clay deposit (Rheinisches Schiefergebirge, Germany). Appl. Clay Sci. 10, 231–245.
Dill, H.G., Bosse, H.-R., Henning, K.-H., Fricke, A., Ahrend, H., 1997. Mineralogical and chemical variations in hypogene and supergene kaolin deposits in a mobile fold belt—the Central Andes of northwestern Peru. Mineral. Deposita 32, 149–163.
Dill, H.G., Sachsenhofer, R., Grecula, P., Sasvari, T., Palinkas, L., Borojevic-Sostaric, S., Strmic-Palinkas S., Prochaska, W., Garuti, G., Zaccarini, F., Arbouille, D., Schulz H., Schmidt, B., Locmelis, B., 2008a. The origin of mineral and energy resources of Central Europe (map 1: 2500000). Geological Society of London, London (on CD ROM).
Dill, H.G., Sachsenhofer, R., Grecula, P., Sasvari, T., Palinkas, L., Borojevic-Sostaric, S., Strmic-Palinkas, S., Prochaska, W., Garuti, G., Zaccarini, F., Arbouille, D., Schulz, H., 2008b. Fossil fuels, ore and industrial minerals. In: McCann, T. (Ed.), Geology of Central Europe. Geological Society of London, Special Publication, London, pp. 1341–1449.
Dill, H.G., Gerdes, A., Weber, B., 2010. Age and mineralogy of supergene uranium minerals — tools to unravel geomorphological and palaeohydrological processes in granitic terrains (Bohemian Massif, SE Germany). Geomorphology 117, 44–65.
Dill, H.G., Dohrmann, R., Kaufhold, S., Balaban, S.-I., 2015. Kaolinization — a tool to unravel the formation and unroofing of the Pleystein pegmatite–aplite system (SE Germany). Ore Geol. Rev. 69, 33–56.
Domínguez, E.A., Iglesias, C., Dondi, M., Murray, H.H., 2010. Genesis of the La Espingarda kaolin deposit in Patagonia. Appl. Clay Sci. 47, 290–302.
Duke, E.F., 1994. Near infrared spectra of muscovite, Tschermak substitution, and metamorphic reaction progress: implications for remote sensing. Geology 22, 621–624.
Elzea Kogel, J., 2002. Kaolin Mineralogy, Quality and Major Markets in the Georgia Kaolins: Geology and Utilization. Society for Mining, Metallurgy and Exploration, USA (96 pp.).
Fernández-Caliani, J.C., Galán, E., Aparicio, P., Miras, A., Márquez, M.G., 2010. Origin and geochemical evolution of the Nuevo Montecastelo kaolin deposit (Galicia, NW Spain). Appl. Clay Sci. 49, 91–97.
Galloway, W.E., Hobday, D.K., 1996. Terrigenous Clastic Depositional Systems: Applications to Fossil Fuel and Groundwater Resources. Springer, Berlin (489 pp.).
Galos, K., 2010. Ball clays for the production of porcelain tiles in Poland. Gospodarka Surowcami Mineralnym 26, 21–43.
Gilg, A., 2000. D–H evidence for the timing of kaolinization in Northeast Bavaria, Germany. Chem. Geol. 170, 5–18.
Giral-Kacmarćik, S., Savin, S.M., Nahon, D.B., Girard, J.-P., Lucas, Y., Abel, L.J., 1998. Oxygen isotope geochemistry of kaolinite in laterite-forming processes, Manaus, Amazonas, Brazil. Geochim. Cosmochim. Acta 62, 1865–1879.
Göd, R., Brandstätter, F., 1999. Evidence for gold-bearing propylitized Hercynian granites, Moldanubicum, South Bohemian Massif, Austria. Berg-Huttenmann. Monatsh. 144, 470–475.
Grecco, L.E., Marfil, S.A., Maiza, P.J., 2012. Mineralogy and geochemistry of hydrothermal kaolins from the Adelita mine, Patagonia (Argentina); relation to other mineralization in the area. Clay Miner. 47, 131–146.
Gudden, H., 1975. Zur Bleiführung in Trias-Sedimenten der nördlichen Oberpfalz. Geol. Bavarica 74, 33–55.
Günzler, H., Gremlich, H.-U., 2003. IR-Spektroskopie. Wiley, VCH, Weinheim (365 pp.).
Harben, P.W., Kužvart, M., 1997. Industrial Minerals: A Global Geology. Industrial Minerals Information Limited, Worcester Park (462 pp.).
Harris, C., Compton, J.S., Bevington, S.A., 1999. Oxygen and hydrogen isotope composition of kaolinite deposits, Cape Peninsula, South Africa; low-temperature, meteoric origin. Econ. Geol. 94, 1353–1366.
Haunschild, H., 1979. Die Bohrungen Neudorf b. Luhe A und B und ihre geologischen Befunde. Geol. Bl. Nordost Bayern 29, 147–166.
Haunschild, H., Salger, M., 1987. Die Trias in der Kernbohrung Wackersdorf 1/Opf. (Vorläufige Mitteilung). Geol. Bl. NO-Bayern 37, 23–46.
Herrmann, W., Blake, M., Doyle, M., Huston, D., Kamprad, J., Merry, N., Pontual, S., 2001. Short wavelength infrared (SWIR) spectral analysis of hydrothermal alteration zones associated with base metal sulfide deposits at Rosebery and Western Tharsis, Tasmania, and Highway-Reward, Queensland. Econ. Geol. 96, 939–955.
Heim, F., 1936. Die nutzbaren Gesteine und Erden Bayerns vol. 2, 132–217. Bayerisches Oberbergamt, München.
Hornung, J., Aigner, T., 2002. Reservoir architecture in a terminal alluvial plain: an outcrop analogue study (Upper Triassic, Southern Germany). Part I: Sedimentology and petrophysics. J. Pet. Geol. 25, 3–30.
Huckenholz, H.G., Kunzmann, T., 1993. Tertiärer Vulkanismus im bayerischen Teil des Egergrabens und des mesozoischen Vorlandes. Beih. Eur. J. Mineral. 5, 1–34.
Johan, Z., Johan, V., 2005. Accessory minerals of the Cínovec (Zinnwald) granite cupola, Czech Republic: indicators of petrogenetic evolution. Mineral. Petrol. 83, 113–150.
John, C.M., Banerjee, N.R., Longstaffe, F.J., Sica, C., Law, K.R., Zachos, J.C., 2012. Clay assemblage and oxygen isotopic constraints on the weathering response to the Paleocene–Eocene thermal maximum, east coast of North America. Geology 40, 591–594.
Kadir, S., Erkoyun, H., 2013. Genesis of the hydrothermal Karaçayır kaolinite deposit in Miocene volcanics and Palaeozoic metamorphic rocks of the Uşak-Güre Basin, western Turkey. Turk. J. Earth Sci. 22, 444–468.
Kendall, A.C., 1992. Evaporites. In: Walker, R.G., James, N.P. (Eds.), Facies Models—Response to Sea Level Change. Geological Association Canada, pp. 375–409.
Knetsch, G., 1929. Der Keuper in der bayerischen Oberpfalz. N. Jb. Mineral. 61, 83–150.
Kogure, T., Inoue, A., Beaufort, D., 2005. Polytype and morphology analyses of kaolin minerals by electron back-scattered diffraction. Clay Clay Miner. 53, 201–210.
Koneshloo, M., Vinches, M., Rolley, J.P., 2005. Modelling the sedimentary deposits of kaolin clays in continental environments: application to the Charentes deposits, France. 20th World Mining Congress, pp. 375–384.
Köster, H., 1974. Ein Beitrag zur Geochemie und Enstehung der oberpfälzischen Kaolin-Feldspat-Lagerstätten. Geol. Rundsch. 63, 655–689.
Kostov, I., Kostov, R.I., 1999. Crystal habits of minerals. Bulg. Acad. Monogr. 1, 1–415.
Kräuter, R., 2012. Kaolin with reduced content of inorganic compounds containing phosphorous, production and use. Patent EP 2423266 A2.
Kromer, H., 1980. Clays and clay minerals in the Federal Republic of Germany. Geol. Jahrb. 39, 25–45.
Kužvart, M., 1968. Kaolin deposits of Czechoslovakia. International Geological Congress, 23th Prague, 1968 Proceedings 15, pp. 47–73.
Lanson, B., Beaufort, D., Berger, G., Bauer, A., Cassagnabere, A., Meunier, A., 2002. Authigenic kaolin and illite minerals during burial diagenesis of sandstones: a review. Clay Miner. 37, 1–22.
Lorenz, V., Gwosdz, W., 1997. Bewertungskriterien für Industriemineral, Steine und Erden, part 1 Tone. Geol. Jahrb. H 2, 1–108.
Marfil, S.S., Maiza, P.J., Cardellach, E., Corbella, M., 2005. Origin of kaolin deposits in the "Los Menucos" area, Rio Negro Province, Argentina. Clay Miner. 40, 283–293.
Matte, P., 2001. The Variscan collage and orogeny (480 ± 290 Ma) and the tectonic definition of the Armorica microplate: a review. Terra Nova 13, 122–128.
McAulay, G.E., Burley, S.D., Fallick, A.E., Kusznir, N.J., 1994. Palaeohydrodynamic fluid flow regimes during diagenesis of the Brent Group in the Hutton–NW Hutton reservoirs: constraints from oxygen isotope studies of authigenic kaolin and reverse flexural modeling. Clay Miner. 29, 609–626.
Meier, L.P., Kahr, G., 1999. Determination of the cation exchange capacity (CEC) of clay minerals using the complexes of copper (II) ion with triethylenetetramine and tetraethylenepentamine. Clay Clay Miner. 47, 386–388.
Melchiorre, E.B., Williams, P.A., Bevins, R.E., 2001. A low temperature oxygen isotope thermometer for cerussite, with applications at Broken Hill, new South Wales, Australia. Geochim. Cosmochim. Acta 65, 2527–2533.
Merriman, R.J., Peacor, D.R., 1999. Very low-grade metapelites; mineralogy, microfabrics and measuring reaction progress. In: Frey, M., Robinson, D. (Eds.), Low-Grade Metamorphism. Blackwell Sciences Ltd., Oxford, pp. 10–60.
Meyer, R.K.F., Mielke, H., 1993. Erläuterungen zur Geologischen Karte von Bayern 1:25000 Blatt Nr. 6639 Wackersdorf, BGLA 194 pp.
Meyer, R.K.F., Schmidt-Kaler, H., 1996. Jura.- In: Freudenberger W. and Schwerd, K. (eds.) Erläuterungen zur Geologischen Karte von Bayern 1:500,000 (4th edition) Bayerisches Geologisches Landesamt, 90–111.
Miall, A.D., 1977. A review of the braided river depositional environment. Earth-Sci. Rev. 13, 1–62.
Miall, A.D., 1992. Alluvial deposits. In: Walker, R.G., James, N.P. (Eds.), Facies Models: Response to Sea Level Change. Geological Association of Canada, St John's, Newfoundland, pp. 119–142.
Miall, A.D., 1994. Reconstructing fluvial macroform architecture from two-dimensional outcrops: examples from the Castlegate Sandstone, Book Cliffs, Utah. J. Sediment. Res. B64, 146–158.
Miall, A.D., 1996. The Geology of Fluvial Deposits. Springer-Verlag, New York (582 pp.).
Miall, A.D., 1999. Principles of Sedimentary Basin Analysis. 3rd ed. Springer, Berlin (616 pp.).
Murray, H.H., 2000. Traditional and new applications for kaolin, smectite, palygorskite: a general overview. Appl. Clay Sci. 17, 207–221.
Murray, H.H., 2007. Applied clay mineralogy. Occurrences, processing and application of kaolins, bentonites, palygorskite–sepiolite and common clays. Dev. Clay Sci. 2, 1–188.

Parnell, J., Baron, M., Boyce, A., 2000. Controls on kaolinite and dickite distribution, Highland Boundary Fault Zone, Scotland and Northern Ireland. J. Geol. Soc. Lond. 157, 635–640.
Pirajno, F., Burlow, R., Huston, D., 2010. The Magellan Pb deposit, Western Australia; a new category within the class of supergene non-sulfide mineral systems. Ore Geol. Rev. 37, 101–113.
Psyrillos, A., Manning, D.A.C., Burley, S.D., 1998. Geochemical constraints on kaolinization in the St. Austell granite, Cornwall, England. J. Geol. Soc. Lond. 155, 829–840.
Pupin, J.P., 1980. Zircon and granite petrology. Contrib. Mineral. Petrol. 73, 207–220.
Raumer von, J.F., Stampfli, G.M., Bussy, F., 2003. Gondwana-derived microcontinents — the constituents of the Variscan and Alpine collision orogens. Tectonophysics 365, 7–22.
Reinhard, L., Ricken, W., 2000. Climate cycles documented in a playa system: comparison of geochemical signatures derived from subbasins (Triassic, Middle Keuper, German Basin). In: Bock, H., Müller, R., Swennen, R., Zimmerle, W. (Eds.), West European Case Studies in Stratigraphy. Zentralblatt für Geologie und Paläontologie part I 1999, pp. 315–340.
Richter, D.K., Gorgen, P., Gotte, T., 2008. Monazite cathodoluminescence — a new tool for heavy mineral analysis of siliciclastic sedimentary rocks. Sediment. Geol. 209, 36–41.
Ruiz Cruz, M.D., Reyes, E., 1998. Kaolinite and dickite formation during shale diagenesis: isotopic data. Appl. Geochem. 13, 95–104.
Russell, J.D., Fraser, A.R., 1994. Infrared methods. In: Wilson, M.J. (Ed.), Clay Mineralogy: Spectroscopic and Chemical Determinative Methods. Chapman and Hall, London, pp. 11–67.
Salama, R.B., 1997. Geomorphology, geology and palaeohydrology of the broad alluvial valleys of the Salt River System, Western Australia. Aust. J. Earth Sci. 44, 751–765.
Salger, M., 1958. Mineralogisch und sedimentpetrographische Untersuchungen am Kaolinprofil der Bohrung Kick Nr. 9 bei Schnaittenbach/Opf. Geologica Bavarica 37 pp. 1–84.
Salger, M., 1979. Die Bohrungen Neudorf b. Luhe A und B: Mineralogische Untersuchungsergebnisse. Geol. Bl. NO-Bayern 29, 167–170.
Schroeder, P.A., Shiflet, J., 2000. Ti-bearing phases in the Huber Formation, an East Georgia kaolin deposit. Clay Clay Miner. 48, 151–158.
Scott, P.W., Bristow, C.M., 2002. Industrial Minerals and Extractive Industry Geology. Geological Society (376 pp.).
Selley, R.C., 2000. Applied Sedimentology. 2nd ed. Academic Press (523 pp.).
Sheppard, S.M.F., 1977. The Cornubian batholith, SW England: D/H and $^{18}O/^{16}O$ studies of kaolinite and other alteration minerals. J. Geol. Soc. 133, 573–591.
Siebel, W., Blaha, U., Chen, F., Rohrmüller, J., 2005. Geochronology and geochemistry of a dyke–host rock association and implications for the formation of the Bavarian Pfahl shear zone, Bohemian Massif. Int. J. Earth Sci. 94, 8–23.
Siehl, A., Thein, I., 1989. Minette-type ironstones. In: Young, T.P., Taylor, W.E.G. (Eds.), Phanerozoic Ironstones. British Geological Society Special Publication 46, pp. 175–193.
Stahl, A., 1912. Die Verbereitung der Kaolinlagerstätten in Deutschland. Archiv f. Lagerstättenforschung 12, 1–135.
Steinlein, H., 1939. Neue Arbeitsergebnisse in der Oberpfälzer Trias. Z. Dtsch. Geol. Ges. 91, 778–779.
Störr, M., 2002. Kaolin-Ton-Feldspatbergbau und Keramik-Industrie der Oberpfalz. Verlag Störr, Ostklüne (99 pp.).
Störr, M., 2006. Zur Geologie und Genese der Kaoline des Böhmischen Massivs. Z. Geol. Wiss. 34, 389–421.
Störr, M., Köster, H.M., Kromer, H., Hilz, M., 1991. Minerale der Crandallit-Reihe im Kaolin von Hirschau-Schnaittenbach, Oberpfalz. Z. Geol. Wiss. 19, 677–683.
Szczerba, M., Sawłowicz, Z., 2009. Remarks on the origin of cerussite in the Upper Silesian Zn–Pb deposits, Poland. Mineralogia 40, 54–64.
Tillmann, H., 1940. Ergebnisse der geologischen Aufnahme der Freihunger Störungszone, Blatt Kaltenbrunn Nr. 166 (Oberpfalz). Z. Dtsch. Geol. Ges. 92, 541–564.
Tucker, M., 2001. Sedimentary Petrology. Blackwell, London (262 pp.).
Twidale, C.R., 2002. The two-stage concept of landform and landscape development involving etching. origin, development and implications of an idea. Earth-Sci. Rev. 57, 37–74.
Warren, J.K., 2010. Evaporites through time: tectonic, climatic and eustatic controls in marine and nonmarine deposits. Earth Sci. Rev. 98, 217–268.
Weaver, C.E., 1989. Clays, Muds, and Shales. Elsevier, Amsterdam (819 pp.).
Wilson, I.R., Jiranek, J., 1995. Kaolin deposits of the Czech Republic and some comparisons with South-West England. Read at the Annual Conference of the Ussher Society 1995, pp. 357–362.
Zitzmann, A., 1981. Geologische Übersichtskarte 1: 200000 CC 6334 Bayreuth. Bundesanstalt für Geowissenschaften und Rohstoffe, Hannover.